JACS
JOURNAL OF THE AMERICAN CHEMICAL SOCIETY
pubs.acs.org/JACS
Article

Substituent Effects on Exchange Coupling and Magnetic Relaxation in 2,2′-Bipyrimidine Radical-Bridged Dilanthanide Complexes

Colin A. Gould, Edward Mu, Veacheslav Vieru, Lucy E. Darago, Khetpakorn Chakarawet, Miguel I. Gonzalez, Selvan Demir, and Jeffrey R. Long*

Cite This: https://dx.doi.org/10.1021/jacs.0c10612

ABSTRACT: Systematic analysis of related compounds is crucial to the design of single-molecule magnets with improved properties, yet such studies on multinuclear lanthanide complexes with strong magnetic coupling remain rare. Herein, we present the synthesis and magnetic characterization of the series of radical-bridged dilanthanide complex salts $[(Cp^*_2Ln)_2(\mu\text{-}5,5'\text{-}R_2bpym)](BPh_4)$ (Ln = Gd, Dy; R = NMe_2 (**1**), OEt (**2**), Me (**3**), F (**4**); bpym = 2,2′-bipyrimidine). Modification of the substituent on the bridging 5,5′-R_2bpym radical anion allows the magnetic exchange coupling constant, J_{Gd-rad}, for the gadolinium compounds in this series to be tuned over a range from −2.7 cm^{-1} (**1**) to −11.1 cm^{-1} (**4**), with electron-withdrawing or -donating substituents increasing or decreasing the strength of exchange coupling, respectively. Modulation of the exchange coupling interaction has a significant impact on the magnetic relaxation dynamics of the single-molecule magnets **1-Dy** through **4-Dy**, where stronger J_{Gd-rad} for the corresponding Gd^{3+} compounds is associated with larger thermal barriers to magnetic relaxation (U_{eff}), open magnetic hysteresis at higher temperatures, and slower magnetic relaxation rates for through-barrier processes. Further, we derive an empirical linear correlation between the experimental U_{eff} values for **1-Dy** through **4-Dy** and the magnitude of J_{Gd-rad} for the corresponding gadolinium derivatives that provides insight into the electronic structure of these complexes. This simple model applies to other organic radical-bridged dysprosium complexes in the literature, and it establishes clear design criteria for increasing magnetic operating temperatures in radical-bridged molecules.

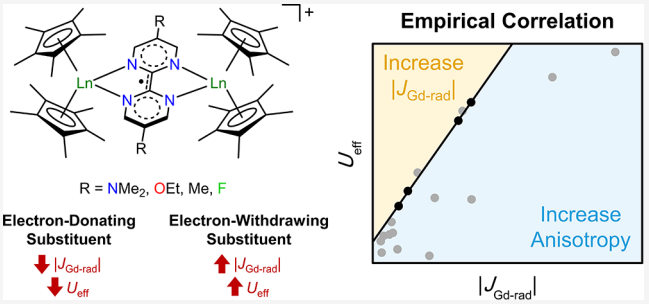

INTRODUCTION

Single-molecule magnets exhibit slow magnetic relaxation that is of molecular origin, arising from the presence of a bistable magnetic ground state with a thermal barrier to inversion of the magnetic moment (U).[1,2] When $k_BT \ll U$, many such molecular compounds have been shown to exhibit magnetic hysteresis, a property that could potentially be utilized in applications such as nanoscale information storage or spin-based computing.[3−6] However, the vast majority of single-molecule magnets retain their magnetic memory only at prohibitively low temperatures. Significant research has therefore focused on increasing the maximum operating temperature, which is typically defined as the temperature at which the magnetic relaxation time, τ, is equal to 100 s (T_b or blocking temperature) or the highest temperature at which magnetic hysteresis is observed.[2] Higher operating temperatures can be achieved by maximizing the effective thermal barrier to magnetic relaxation (U_{eff}), which typically sets an upper limit to the value of T_b, and by mitigating through-barrier relaxation pathways, such as quantum tunnelling of the magnetization.[7,8]

Over the past decade, the most significant advances in enhancing the operating temperatures of single-molecule magnets have been made with lanthanide-based systems.[9,10] These breakthroughs have been enabled in part by the development of clear design criteria for achieving large values of U_{eff} in mononuclear lanthanide complexes.[11−15] For example, increasing the axiality of the ligand field for oblate Dy^{3+} and Tb^{3+} ions leads to larger thermal barriers.[11] Systematic studies conducted on related complexes have been crucial in identifying these design principles and in verifying their predictions.[16−18] Importantly, these criteria link magnetic properties to molecular structure, which can be easily elucidated through experimental methods such as single-crystal X-ray diffraction, thereby providing a facile method to identify promising single-molecule magnet candidates. For instance, the use of a sterically encumbered pentaisopropylcyclopentadienyl ligand (Cp^{iPr5}) and a pentamethylcyclopentadienyl ligand (Cp*) in $[DyCp^*Cp^{iPr5}]^+$ gives rise to shorter Ln−Cp

Received: October 6, 2020

Scheme 1. Synthesis of the Radical-Bridged Dilanthanide Compounds $[(Cp^*_2Ln)_2(\mu\text{-}5,5'\text{-}R_2bpym)](BPh_4)$ (Ln = Gd, Dy; R = NMe_2 (1), OEt (2), Me (3), F (4))

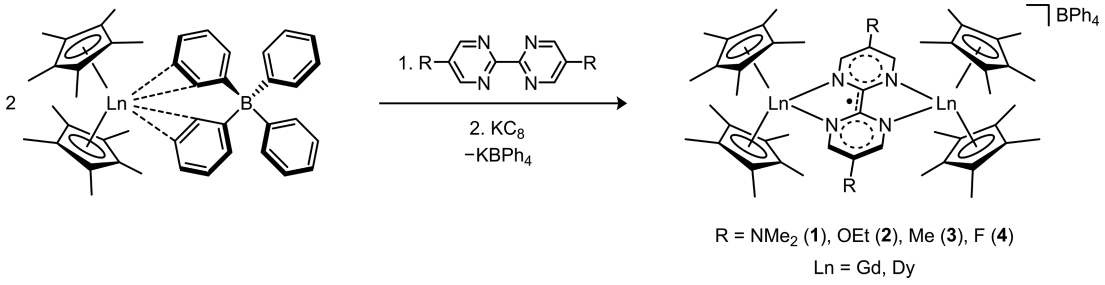

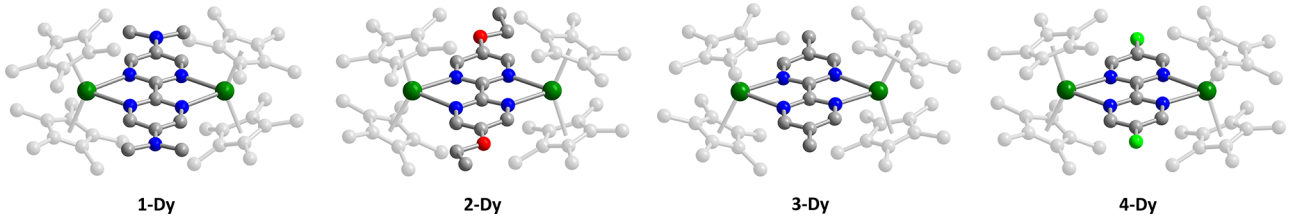

Figure 1. Crystal structures of the complex cations in $[(Cp^*_2Dy)_2(\mu\text{-}5,5'\text{-}R_2bpym)](BPh_4)$ (R = NMe_2 (**1**), OEt (**2**), Me (**3**), F (**4**)). Dark green, gray, blue, red, and lime green spheres represent Dy, C, N, O, and F atoms, respectively; H atoms are omitted for clarity.

bond distances and a larger Cp−Ln−Cp angle than analogous $[DyCp^R_2]^+$ complexes,[19−21] resulting in greater axial anisotropy and a 100-s magnetic blocking temperature of 65 K, the highest value yet reported for any molecule.[22]

Multinuclear lanthanide complexes featuring radical bridging ligands also display some of the highest operating temperatures yet reported for single-molecule magnets, as high as T_b = 20 K.[23] A small but growing number of these compounds has emerged following the discovery of very strong magnetic exchange in $[(\{N(SiMe_3)_2\}_2(THF)Ln)_2(\mu\text{-}N_2)]^-$ (Ln = Gd, Tb, Dy).[24,25] For these molecules with strong coupling, both single-ion anisotropy and magnetic exchange interactions between the lanthanide and bridging radical dictate the magnitude of the thermal barrier to magnetic relaxation.[26] These properties are difficult to experimentally quantify for anisotropic lanthanide ions, and they can require intensive calculations to theoretically predict.[27,28] As a result, identifying whether anisotropy or exchange limits the value of U_{eff} can be quite challenging, thus forestalling the design of molecules with improved magnetic properties. Toward this end, the systematic analysis of related radical-bridged complexes with well-defined structural or electronic differences stands as an important goal in the field of molecular magnetism. Nevertheless, such studies on radical-bridged complexes remain rare, in contrast to the numerous studies on series of multinuclear lanthanide or transition metal complexes with diamagnetic bridging ligands.[29−34]

Herein, we report the synthesis and detailed magnetic characterization of the series of organic radical-bridged dilanthanide complex salts $[(Cp^*_2Ln)_2(\mu\text{-}5,5'\text{-}R_2bpym)](BPh_4)$ (Ln = Gd, Dy; R = NMe_2(**1**), OEt (**2**), Me (**3**), F (**4**)). Modification of the substituent on 5,5′-R_2bpym radical anion induces dramatic changes in the magnitude of the intramolecular magnetic exchange, with electron-donating and -withdrawing substituents decreasing and increasing the magnitude of the exchange coupling constant (J_{Ln-rad}), respectively, as quantified for the gadolinium congeners. Significantly, a linear correlation is demonstrated between the experimental U_{eff} values for **1-Dy** through **4-Dy** and $|J_{Gd-rad}|$ of the corresponding gadolinium derivatives. This empirical relation can be extended to other organic radical-bridged dysprosium compounds in the literature and brings into focus key design principles to access molecules in this class with larger U_{eff} values and higher operating temperatures.

RESULTS AND DISCUSSION

Synthesis and Structural Characterization. The molecule 2,2′-bipyrimidine (bpym) serves as an ubiquitous bridging ligand in coordination chemistry, however, symmetric 5,5′-R_2bpym variants have only yet been reported for alkyl, aryl, ether, and bromine substituents.[35−38] Bipyrimidine derivatives are typically synthesized via Cu- or Ni-mediated coupling reactions, and therefore the synthesis of 5,5′-R_2bpym was first attempted via a Ni-catalyzed homocoupling of the corresponding 5-R-2-chloropyrimidine.[39−41] This approach furnished 5,5′-R_2bpym with electron-donating substituents R = Me, OEt, and NMe_2 in isolated yields between 33 and 37% but did not yield electron-deficient derivatives with R = F or CF_3. These results are consistent with reports of the synthesis of 5,5′-R_2bpy (bpy = 2,2′-bipyridine), which found lower yields for the Ni-catalyzed homocoupling of 5-R-2-chloropyridine substrates bearing electron-withdrawing substituents.[42−44] Attempts to synthesize derivatives with R = F or CF_3 via Cu-mediated homocoupling reactions were also unsuccessful. Instead, a Stille reaction[45,46] was used to couple 5-fluoro-2-tributylstannylpyrimidine and 5-fluoro-2-chloropyrimidine, affording 5,5′-F_2bpym in 57% isolated yield. Although it was not possible in our hands to isolate 5,5′-$(CF_3)_2$bpym by an analogous route, the Pd-catalyzed coupling of 5-trifluoromethyl-2-chloropyrimidine with 5-fluoro-2-tributylstannylpyrimidine furnished 5,5′-F(CF_3)bpym in 46% isolated yield.

Analogous to the synthesis of the radical-bridged lanthanide complex salts $[(Cp^*_2Ln)_2(\mu\text{-bpym})](BPh_4)$,[47] reaction of $[Cp^*_2Ln](BPh_4)$ with 5,5′-R_2bpym, followed by reduction with potassium graphite, gave the compounds $[(Cp^*_2Ln)_2(\mu\text{-}5,5'\text{-}R_2bpym)](BPh_4)$ (R = NMe_2 (**1**), OEt (**2**), Me (**3**), and F (**4**); Ln = Gd, Dy) in 27−69% isolated yield (Scheme 1). A mixture of THF and toluene was used as the reaction solvent

https://dx.doi.org/10.1021/jacs.0c10612
J. Am. Chem. Soc. XXXX, XXX, XXX−XXX

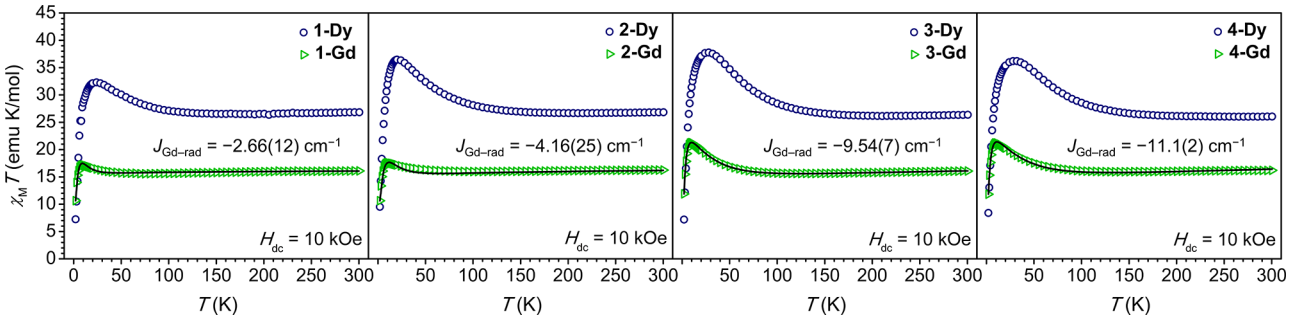

Figure 2. Dc magnetic susceptibility data for **1**−**4** under an applied magnetic field of 10 kOe. The black lines represent fits to the data for **1-Gd** through **4-Gd**, as described in the main text, corresponding to a 4-fold increase in J_{Gd-rad} across the series.

in the synthesis of **1**−**3**, but these conditions did not afford the desired compounds with 5,5′-F_2bpym or 5,5′-F(CF_3)bpym. Given the electron-deficient nature of the fluoro- and trifluoromethyl-substituted ligands, it is likely that these ligands coordinate more weakly to lanthanide ions, and thus the presence of coordinating solvent may hinder complex formation. Exclusion of THF from the reaction and crystallization conditions enabled isolation of **4**, although attempts to isolate compounds with 5,5′-F(CF_3)bpym, the most electron-deficient ligand in the series, were not successful.

The solid-state structures of compounds **1**−**4** were determined from single-crystal X-ray diffraction data (Figure 1) with the exception of **1-Gd**, for which sufficient quality single crystals could not be obtained. The C(2)−C(2′) bond distance in a bpym ligand is indicative of its charge state,[48] and the corresponding distances in **1**−**4** range from 1.403(14) to 1.432(18) Å, consistent with previously reported bpym$^{\bullet-}$ complexes.[47,49,50] The average Dy−N and Gd−N bond distances range from 2.424(6) to 2.440(6) Å and 2.458(2) to 2.469(5) Å, respectively, consistent with the average Ln−N bond distances in [(Cp*$_2$Dy)$_2$(μ-bpym)](BPh$_4$) (data for [(Cp*$_2$Gd)$_2$(μ-bpym)](BPh$_4$) were consistently low resolution and were not published as a result).[47] Complexes **1**−**4** show average Dy−C and Gd−C distances of 2.627(19) and 2.649(12) Å, respectively, and average Cp−Dy−Cp and Cp−Gd−Cp angles of 140.1(3)° and 139.2(4)°, respectively, consistent with [(Cp*$_2$Dy)$_2$(μ-bpym)](BPh$_4$).[47] The large uncertainties in these values arise from positional disorder of the pentamethylcyclopentadienyl ligands. The Dy−C bond distances and Cp−Dy−Cp angles in **1**−**4** are similar to those reported previously for single-molecule magnets that contain Cp*$_2$Dy units, which typically display high single-ion anisotropy due to the strong axial ligand field exerted by the cyclopentadienyl ligands.[51] The axis defined by the two lanthanide centers in **1**−**4** is nearly parallel with the plane of the 5,5′-R_2bpym ligand (defined by the 12 atoms of the bipyrimidine fragment), deviating by only 0.6(1)° to 3.5(1)°. Overall, the bond distances and angles in **1**−**4** are similar across the series and follow no recognizable trend, suggesting that any differences in the magnetic properties of these compounds can be attributed to the electronic influence of the substituent on the 5,5′-R_2bpym ligand.

Magnetic Exchange Coupling. Dc magnetic susceptibility data were initially collected for **1**−**4** from 2 to 300 K under an applied magnetic field of 1 kOe (see section S5.1 of the Supporting Information). At this field, the values of $\chi_M T$ at 300 K for the Gd^{3+} congeners range from 16.3 to 17.3 emu K/mol, slightly greater than the theoretical value of 16.1 emu K/mol predicted for two noninteracting Gd^{3+} centers and an S = 1/2 organic radical. This discrepancy is due to contributions from temperature-independent paramagnetism, which is suppressed under a 10 kOe field (Figure 2), resulting in $\chi_M T$ values of 16.1 to 16.2 emu K/mol for **1-Gd** through **4-Gd** at 300 K. As the temperature is lowered, $\chi_M T$ passes through a shallow minimum between 75 and 140 K before rising to a maximum value ranging from 18.6 to 23.3 emu K/mol (under a 1 kOe field), indicative of antiferromagnetic exchange coupling between the Gd^{3+} centers and bpym$^{\bullet-}$. These maximum $\chi_M T$ values approach the theoretical value of 24.4 emu K/mol for an S = $^{13}/_2$ system resulting from intramolecular antiferromagnetic Gd^{3+}−ligand radical exchange coupling.

The $\chi_M T$ data for **1-Dy** through **4-Dy** exhibit qualitatively similar behavior to those of the Gd compounds (see section S5.1 of the Supporting Information and Figure 2). Under a 10 kOe field, the $\chi_M T$ values at 300 K range from 26.3 to 28.6 emu K/mol, slightly lower than the theoretical value of 28.7 emu K/mol for two noninteracting Dy^{3+} centers and an S = 1/2 organic radical. As the temperature is lowered, the $\chi_M T$ curves rise to maxima between 32.3 and 37.1 emu K/mol, indicative of the formation of a high-angular momentum ground state arising from magnetic exchange. The peak in $\chi_M T$ is followed by a precipitous drop at even lower temperatures, indicative of magnetic blocking.

The magnitude of the exchange coupling interaction was quantified for compounds of isotropic Gd^{3+} (4f^7) by fitting the dc susceptibility data to the following spin-only Hamiltonian: $\hat{H} = -2J_{Gd-rad}\hat{S}_{rad}(\hat{S}_{Gd(1)} + \hat{S}_{Gd(2)})$, where J_{Gd-rad} is the exchange constant corresponding to intramolecular Gd^{3+}−bpym$^{\bullet-}$ coupling, $\hat{S}_{rad}$ is the spin operator for bpym$^{\bullet-}$, and $\hat{S}_{Gd(n)}$ is the spin operator for each Gd^{3+} ion (see Figure 2 and S40, S43, S45, and S47). Terms that account for temperature-independent paramagnetism and intermolecular exchange interactions were also included in the fits of all data (see Tables S8−S11). Corresponding fits of the full range of data for **3-Gd** and **4-Gd** under 10 kOe yield J_{Gd-rad} = −9.54(7) and −11.1(2) cm^{-1}, respectively (Figure 2, black lines). The value of J_{Gd-rad} for **4-Gd** is among the largest yet measured for a radical-bridged lanthanide complex and is slightly larger than J_{Gd-rad} = −10 cm^{-1} determined for [(Cp*$_2$Gd)$_2$(μ-bpym)](BPh$_4$).[47] For **1-Gd** and **2-Gd**, a modified Hamiltonian incorporating an additional term for intramolecular Gd^{3+}−Gd^{3+} exchange coupling (J_{Gd-Gd}) was necessary to fit the rise in $\chi_M T$ at low temperatures satisfactorily, yielding J_{Gd-rad} = −2.66(12) and −4.16(25) cm^{-1} and J_{Gd-Gd} = 0.125(8) and 0.145(5) cm^{-1}, respectively, at 10 kOe. Weak ferromagnetic Ln^{3+}···Ln^{3+} exchange coupling has been characterized previously in dilanthanide complexes bridged by 2,2′-

https://dx.doi.org/10.1021/jacs.0c10612
J. Am. Chem. Soc. XXXX, XXX, XXX−XXX

bipyrimidine.[52,53] Fits to the data for **3-Gd** and **4-Gd** using this Hamiltonian yielded $J_{Gd-Gd} < 1 \times 10^{-4}$ cm^{-1} and comparable values of J_{Gd-rad} to those obtained using the aforementioned Hamiltonian which considers only intramolecular Gd^{3+}–$bpym^{\bullet-}$ coupling.

The relative strength of the magnetic exchange coupling interaction in **1-Gd** through **4-Gd** and $[(Cp^*_2Gd)_2(\mu\text{-bpym})](BPh_4)$ follows the trend R = NMe_2 < OEt < Me < H < F, which can be rationalized by considering the effect of the substituent on the 5,5′-$R_2bpym^{\bullet-}$ radical spin density. The singly occupied molecular orbital (SOMO) for $bpym^{\bullet-}$ has coefficients on C(2), C(2′), C(5), C(5′), and the nitrogen atoms,[54,55] and the magnitude of J_{Gd-rad} is influenced primarily by the spin density on nitrogen. Substituents at the 5 and 5′ carbons can influence radical spin density through resonance or inductive effects at all positions that possess coefficients in the 5,5′-$R_2bpym^{\bullet-}$ SOMO. For instance, introducing substituents that are electron-withdrawing by induction, such as fluorine, at the 5 and 5′ carbons decreases the radical coefficient at that position, thereby increasing the radical spin density at C(2), C(2′), and the nitrogen atoms and thus the strength of the magnetic exchange interaction. In contrast, introducing electron-donating substituents at the 5 and 5′ carbons increases the radical coefficient at that position, thereby decreasing spin density at C(2), C(2′), and the nitrogen atoms and the magnitude of J_{Gd-rad}. Accordingly, introducing substituents that are weakly electron-donating by induction, such as methyl, results in a slight decrease in the magnitude of J_{Gd-rad}, while introducing substituents that are strongly electron-donating by resonance, such as dimethylamino or ethoxy, results in a substantial decrease in the magnitude of the coupling constant. Such dramatic substituent effects on radical spin density are supported by previous electron paramagnetic resonance (EPR) characterization of other radical anion species,[56,57] however, additional factors may influence the magnitude of J_{Gd-rad} in **1-Gd** through **4-Gd**, including substituent effects on the energy of the 5,5′-$R_2bpym^{\bullet-}$ SOMO. EPR characterization of diamagnetic Y^{3+} or Lu^{3+} derivatives of **1**–**4** and complementary computational analysis could facilitate a more quantitative model of the substituent effect on magnetic coupling in **1-Gd** through **4-Gd**, and such studies represent a clear step toward generalizing the design principles identified here. While the magnitude of the exchange coupling in **1-Dy** through **4-Dy** is challenging to quantify using the experimental magnetic susceptibility data due to the anisotropic nature of the Dy^{3+} ion, the relative magnitude of the peak in the $\chi_M T$ versus T data and the temperature at which this maximum occurs follow a similar trend as that characterized for the Gd derivatives, suggesting a similar ordering of the exchange coupling strength.

Remarkably, these results demonstrate that the magnitude of the exchange coupling constant in organic-radical bridged dilanthanide systems can be tuned by more than a factor of 4, from −2.66(12) to −11.1(2) cm^{-1}, simply through ligand modification. While prior studies on radical-bridged complexes have shown that large changes in magnetic coupling can be induced by changing the donor atoms of the bridging ligand or through installing ligand substituents that alter the molecular structure of the complex, the substituent effect in **1**–**4** arises from the electronic influence of a substituent at a remote, nonmetal binding site.[58−61] Thus, magnetic coupling can be modulated substantially without significant perturbation of the metal coordination environment. It is important to emphasize that the substituent effect in **1**–**4** is achieved by installing substituents on ligand atoms that possess radical spin density in the $bpym^-$ SOMO. In contrast, a recent study on tetraoxolene radical-bridged diiron complexes showed that substituent modifications at positions lacking radical spin density in the ligand SOMO had no effect on the magnitude of metal–radical exchange.[62] These insights are key toward the development of new and better-performing radical-bridged lanthanide single-molecule magnets. Further, these insights could enable the synthesis of improved single-chain magnets, which show relaxation barriers that increase with J, and bulk magnetic materials, which possess magnetic ordering temperatures that are directly proportional to J.

Thermally Activated Magnetic Relaxation. The low-temperature drop in the static magnetic susceptibility data for **1-Dy** through **4-Dy** are indicative of magnetic blocking, and accordingly ac magnetic susceptibility data were collected to investigate the presence of slow magnetic relaxation in each compound. The data for **1-Dy** show two peaks in the out-of-phase magnetic susceptibility (χ'') in the frequency range of 0.1–1500 Hz between 4.5 and 11 K, indicative of two independent magnetic relaxation processes occurring at these temperatures (Figure S50). Similarly, for **2-Dy** two relaxation processes are present, although one process is clearly dominant within the examined temperature range of 5–12.5 K (Figure S54). In contrast, **3-Dy** and **4-Dy** each exhibit a single χ'' peak in the same frequency range and for temperatures ranging from 9 to 17 K (Figures S56 and S58). Magnetic relaxation times, τ, were extracted from simultaneous fits of the ac susceptibility data for **1-Dy** through **4-Dy** using a generalized Debye model (see section S5.2 of the Supporting Information). Arrhenius plots of inverse temperature versus the natural log of τ for **3-Dy** and **4-Dy**, and for the dominant relaxation processes in **1-Dy** and **2-Dy**, are linear, characteristic of magnetic relaxation via a thermally activated Orbach mechanism (see section S5.4 of the Supporting Information).[63] Accordingly, all data were fit to the equation $\tau^{-1} = \tau_0^{-1} \exp(U_{eff}/k_BT)$, yielding thermal barriers to magnetic relaxation (U_{eff}) of 31, 40, 82, and 93 cm^{-1} for **1-Dy** through **4-Dy**, respectively. For comparison, U_{eff} = 88 cm^{-1} for $[(Cp^*_2Dy)_2(\mu\text{-bpym})](BPh_4)$.[47] Thus, the magnitude of U_{eff} increases with the substituent on the radical ligand in the order NMe_2 < OEt < Me < H < F, following the same trend determined for $|J_{Gd\text{-}rad}|$. Plots of $\ln(\tau)$ versus $1/T$ for the minor relaxation process in **1-Dy** and **2-Dy** are also linear with temperature, and the data could be fit to an Orbach mechanism yielding $U_{eff,2}$ = 46 and 94 cm^{-1}, respectively.

The value of U_{eff} for a radical-bridged lanthanide complex depends on both single-ion anisotropy and exchange coupling interactions. For dinuclear systems featuring lanthanides with large single-ion anisotropy, the exchange interaction can be described by the Ising model,[64] and the splitting of electronic states can be approximated with the following Hamiltonian: $\hat{H} = -2J_{Ln-rad}\hat{S}_{rad}(\hat{J}_{Ln(1)} + \hat{J}_{Ln(2)}) + \Sigma B^0_2 O^0_2(i)$, where J_{Ln-rad} is the exchange constant corresponding to intramolecular Ln^{3+}–radical exchange, $\hat{S}_{rad}$ is the spin operator for the organic radical bridging ligand, $\hat{J}_{Ln(n)}$ is the angular momentum operator for each Ln^{3+} ion, and B^0_2 and O^0_2 are parameters that describe crystal field interactions for each lanthanide.[23,65−67] Excited state energies correspond to multiples of J_{Ln-rad}, and the energy difference between the ground and first excited state, typically defined as U_{eff}, is $15|J_{Dy-rad}|$ for anisotropic radical-bridged dysprosium complexes (Figure 3, left). Indeed, this relationship was recently demonstrated

https://dx.doi.org/10.1021/jacs.0c10612
J. Am. Chem. Soc. XXXX, XXX, XXX−XXX

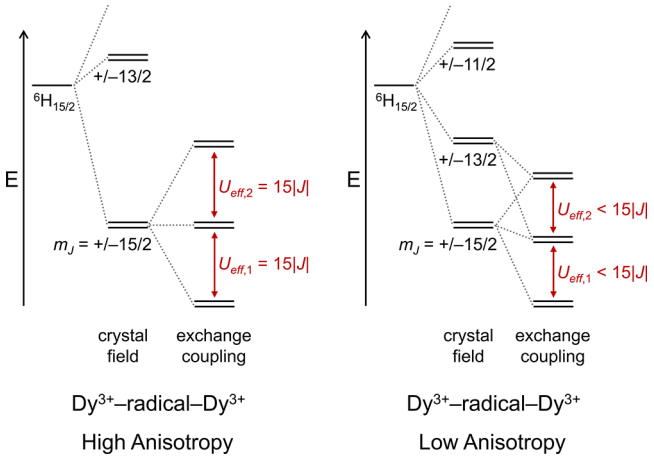

Figure 3. Qualitative energy diagrams for dinuclear radical-bridged dysprosium complexes. The complex on the left displays high single-ion anisotropy and can be described by an Ising model. The complex on the right shows lower single-ion anisotropy and thus the exchange interaction mixes the ground Kramers doublet with the excited doublets, leading to a lower value of U_{eff}.

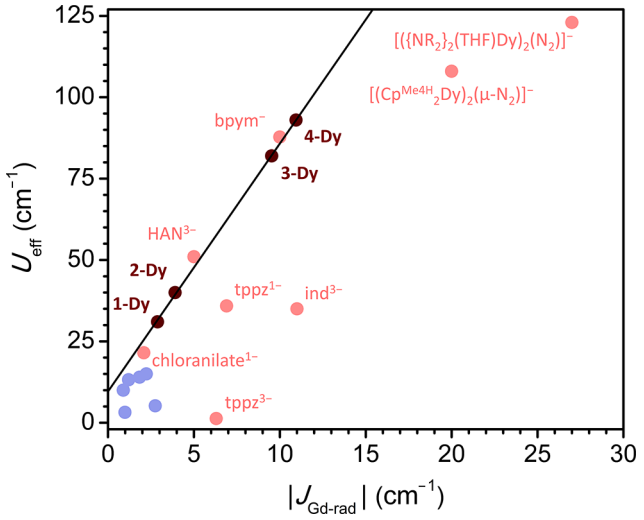

Figure 4. Plot of U_{eff} for **1-Dy** through **4-Dy** versus $|J_{Gd-rad}|$ of the corresponding gadolinium complexes (dark red circles). A linear fit to these data provides an empirical model (black line) with which to analyze the electronic structure of multinuclear radical-bridged compounds (pink circles) and mono- or dinuclear dysprosium complexes featuring a radical ligand which is coupled to one metal center (blue circles). See Table S20 in the Supporting Information for a full list of compounds and references.

experimentally for the N_2^{3-} radical-bridged dysprosium complex $[K(crypt\text{-}222)][(Cp^{Me4H}{}_2Dy)_2(\mu\text{-}N_2)]$ ($[Cp^{Me4H}]^-$ = tetramethylcyclopentadienyl anion).[23] By contrast, a complex with low single-ion anisotropy will possess low-lying crystal field states that are further mixed by the exchange interaction, resulting in a comparatively lower value of U_{eff} (Figure 3, right). Substantial mixing of the crystal field states can also occur for complexes with large single-ion anisotropy and very large values of J_{Ln-rad}.[68] While the Ising model can offer insight into the magnitude of U_{eff} values in radical-bridged lanthanide complexes, its utility is limited due to the difficulty of experimentally determining J_{Ln-rad} for anisotropic lanthanide ions and of quantifying single-ion anisotropy. Indeed, these values are typically obtained through ab initio calculations,[68−70] which can be time-intensive to execute and may possess a wide margin of error.

We accordingly sought to develop an empirical model to rationalize the values of U_{eff} for **1-Dy** through **4-Dy** that does not require determination of J_{Dy-rad}. In particular, the magnitude of magnetic exchange in radical-bridged Gd^{3+} systems has been used as a proxy to estimate the relative magnitude of the exchange coupling in isostructural systems of the anisotropic lanthanides.[23] Given the similar trend in the $\chi_M T$ data for the Dy and Gd congeners of **1** through **4**, we hypothesized that the J_{Gd-rad} values obtained for **1-Gd** through **4-Gd** may directly correlate with the exchange coupling in **1-Dy** through **4-Dy**. Figure 4 features a plot of U_{eff} for the dominant relaxation process in **1-Dy** through **4-Dy** versus $|J_{Gd-rad}|$ for the corresponding Gd compounds (see also Table S20). The resulting plot is linear, which implies that the Dy molecules can be described by an Ising model—that is, U_{eff} is directly proportional to $|J_{Gd-rad}|$ for this series. This observation is consistent with the large single-ion anisotropy reported for other dysprosium complexes with axial Cp* ligands.[51] A linear dependence of U_{eff} on $|J_{Dy-rad}|$ was also previously reported for $[Cr_2Dy_2(OMe)_2(RN\{(CH_2)_2OH\}_2)_2(acac)_4(NO_3)_2]$ (R = Me, Et, *n*Bu) (acac$^-$ = acetylacetonate) using computationally determined values for the exchange coupling constants.[71]

The empirical model proposed here for **1** through **4** can be used more broadly to analyze the electronic structure of multinuclear radical-bridged dysprosium complexes in the literature.[26] For instance, values reported for $[(Cp^*{}_2Ln)_2(\mu\text{-bpym})](BPh_4)$ (Ln = Gd, Dy), $(Cp^*{}_2Ln)_3(\mu\text{-HAN})$ (HAN = hexaazatrinaphthylene), and $[CoCp_2][((HBpz_3)_2Ln)_2(\mu\text{-CA})]$ ($HBpz_3$ = hydrotris(pyrazol-1-yl)borate, CA = chloranilate) all fall near the best-fit line describing the relation between U_{eff} and $|J_{Gd-rad}|$ for **1** through **4**, which implies that these complexes can also be described by an Ising model.[47,72,73] By contrast, data for $[(Cp^*{}_2Ln)_2(\mu\text{-tppz})]^{+/-}$ (tppz = 2,3,5,6-tetra(2-pyridyl)pyrazine) and $[(Cp^*{}_2Ln)_2(\mu\text{-ind})]^-$ (ind = indigo) fall well below the line, which suggests that these complexes possess a value of U_{eff} below the Ising limit (i.e., $U_{eff} < |15J_{Dy-rad}|$) due to low single-ion anisotropy.[74,75] This analysis is consistent with the stronger equatorial interactions observed for the Dy^{3+} centers in these complexes. Indeed, ab initio calculations performed on $[(Cp^*{}_2Dy)_2(\mu\text{-ind})]^-$ predict that the ground Kramers doublet for each Dy^{3+} ion is relatively close in energy to the first excited state (ΔE = 71 cm^{-1}), further confirming the low single-ion anisotropy in this complex (Table S23). For comparison, ΔE = ~200 cm^{-1} for **1-Dy** through **4-Dy** (see below and Table S23). Finally, the empirical model presented here for **1** through **4** can also be used to analyze complexes in which a single dysprosium ion interacts with an organic radical (see section S5.5 of the Supporting Information for additional details).

The correspondence between the best-fit line for **1** through **4** and available literature data for other dysprosium and gadolinium pairs suggests that this empirical model may be a useful predictive tool for identifying radical-bridged dysprosium complexes exhibiting enhanced barriers to magnetic relaxation. Indeed, the maximal value of the energetic splitting between the ground and first excited state, which typically represents U_{eff}, can be estimated using only J_{Gd-rad} for the corresponding Gd complex. This model can also afford insight into strategies for increasing the magnitude of the thermal relaxation barrier. For instance, U_{eff} = 35 cm^{-1} for

https://dx.doi.org/10.1021/jacs.0c10612
J. Am. Chem. Soc. XXXX, XXX, XXX−XXX

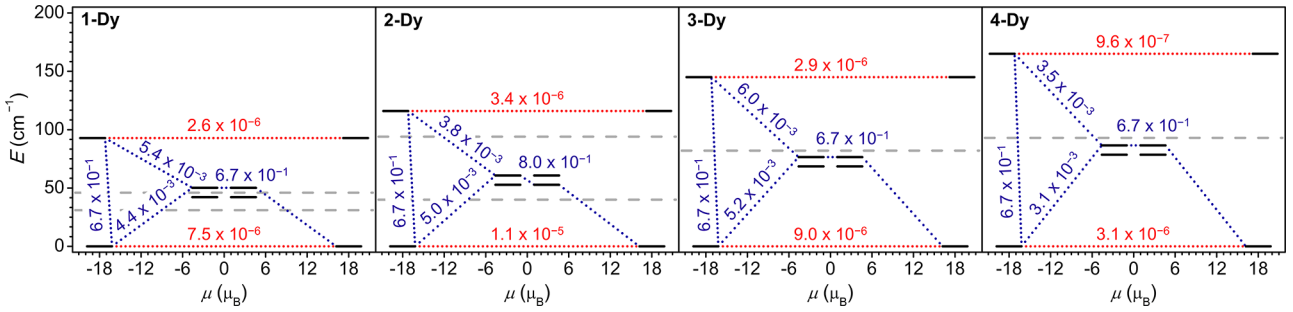

Figure 5. Low-lying exchange spectra calculated for **1-Dy** through **4-Dy**, showing pathways for thermally activated magnetic relaxation (dotted blue lines), quantum tunnelling of the magnetization (dotted red lines), and the experimental U_{eff} or $U_{eff,2}$ values (dashed gray lines). The numbers associated with each path are the largest matrix element connecting each exchange doublet; the square of this value is proportional to the transition rate between states.[68]

$[(Cp^*_2Dy)_2(\mu\text{-ind})]^-$, but the trend presented here indicates that U_{eff} values as large as 93 cm^{-1} could be achieved if the ancillary cyclopentadienyl ligands were modified to maximize the single-ion anisotropy of the Dy^{3+} ions. By contrast, larger energetic splitting between the ground and first excited state will not be accessible simply by modifying the ancillary ligands of the aforementioned HAN-bridged complex, and instead modifications to the radical bridge are needed to increase the magnitude of J_{Dy-rad}. Notably, this empirical model is readily implemented and relies on parameters that can be easily extracted from experimental data, and therefore it could be used to benchmark future computational studies or provide rapid insight into the electronic structure of new radical-bridged complexes.

Two key assumptions are implicit to the foregoing analysis, namely that J_{Gd-rad} is proportional to J_{Dy-rad} and that the proportionality constant relating these two values is the same for all represented complexes. These assumptions appear to be reasonable for complexes in which Dy^{3+} ions interact with organic radicals. In contrast, although the complex $[(Cp^{Me4H}_2Dy)_2(\mu\text{-}N_2)]^-$ does exhibit Ising exchange, it deviates from the trend in Figure 4. This may be due to the strong equatorial ligand field of the N_2^{3-} bridge, which reduces single-ion anisotropy, or due to a change in the proportionality constant that relates J_{Gd-rad} and J_{Dy-rad}, which could result from differences in the exchange mechanism for complexes bridged by N_2^{3-} versus organic radicals.[23] The complex $[(\{N(SiMe_3)_2\}_2(THF)Dy)_2(\mu\text{-}N_2)]^-$ likewise deviates from the model, likely due to low single-ion anisotropy.[24,68] In addition, this model is unlikely to apply to complexes that exhibit low values of $|J_{Gd-rad}|$ (<1 cm^{-1}), wherein single-ion effects are expected to dominate. Clearly, additional studies on series of radical-bridged lanthanide complexes with different organic bridging ligands are necessary to elucidate the generality of the empirical model for **1-Dy** through **4-Dy**.

To provide additional insight into the electronic structure of this series and support for the above analysis, ab initio calculations were performed on **1-Dy** through **4-Dy**. Complete active-space self-consistent field (CASSCF) calculations were carried out to determine the energy of the crystal field states of the individual Dy^{3+} ions in each complex (Table S23), and broken-symmetry density functional theory calculations were used to estimate the strength of the exchange interaction. These calculations predict that the ground Kramers doublet of each Dy^{3+} ion in **1-Dy** through **4-Dy** is well-separated from the first excited doublet (ΔE = ~200 cm^{-1}), consistent with the assumption that these complexes display large single-ion anisotropy and can be described by an Ising model.

The calculated exchange spectra for **1-Dy**, **2-Dy**, **3-Dy**, and **4-Dy** (Figure 5 and Table S25) yield U_{eff} values of 46, 59, 73, and 83 cm^{-1}, respectively, comparable to the experimental U_{eff} values of 31, 40, 82, and 93 cm^{-1}. Interestingly, the separation between the ground state and second excited state in **1-Dy** and **2-Dy** are 93 and 116 cm^{-1}, respectively, which correspond to the $U_{eff,2}$ values of 46 and 94 cm^{-1} determined for the minor relaxation process characterized for each complex. Orbach relaxation via the second excited state has been characterized previously in radical-bridged lanthanide complexes.[23] This mechanism is likely not observed for **3-Dy** and **4-Dy** due to the higher energy of the second excited state in these complexes, which renders an Orbach process thermally inaccessible in the experimental temperature range. Altogether, these calculations confirm that **1-Dy** through **4-Dy** can be described by the Ising model and that the magnitude of U_{eff} for these complexes is dictated by the strength of the exchange coupling.

Through-Barrier Magnetic Relaxation. Dc relaxation measurements were performed on **1-Dy** through **4-Dy** to probe magnetic relaxation dynamics at lower temperatures. For **3-Dy** and **4-Dy**, magnetic relaxation times, τ, were extracted from magnetization versus time plots by fitting the data to a stretched exponential function (see section S5.3 of the Supporting Information). Data for **1-Dy** and **2-Dy** could not be fit accurately by a single stretched exponential function, likely due to the presence of the two independent relaxation processes occurring for each complex. Further attempts to fit the dc relaxation data using a stretched exponential function accounting for two relaxation processes led to overparameterization, and unique fits to the data for **1-Dy** and **2-Dy** could therefore not be obtained.

Plots of $\ln(\tau)$ versus $1/T$ derived from the dc relaxation data for **3-Dy** and **4-Dy** are nonlinear (Figures S81 and S83), indicative of Raman relaxation and quantum tunnelling of the magnetization. Accordingly, the data were fit to the equation $\tau^{-1} = \tau_{tunnel}{}^{-1} + CT^n$, where τ_{tunnel} is the relaxation time for quantum tunnelling and C and n are free variables that describe Raman relaxation, yielding τ_{tunnel} = 660 s, $C = 3.7 \times 10^{-6}$, and n = 3.7 for **3-Dy**, and τ_{tunnel} = 350 s, $C = 2.9 \times 10^{-5}$, and n = 3.0 for **4-Dy**. As τ_{tunnel} values can be influenced by intermolecular dipolar interactions in the solid state, dc relaxation data were also collected on dilute solutions of **3-Dy** (7.8 mM) and **4-Dy** (8.0 mM) in 1,2-difluorobenzene under zero field and 500 Oe (see section S5.3 of the Supporting Information and Figures S82 and S84). Fits to the zero-field data yielded τ_{tunnel} = 94 and

https://dx.doi.org/10.1021/jacs.0c10612
J. Am. Chem. Soc. XXXX, XXX, XXX−XXX

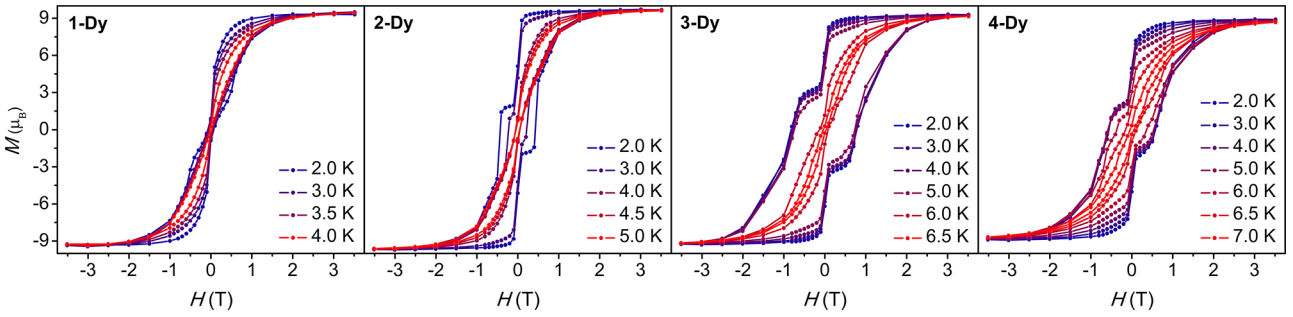

Figure 6. Variable-field magnetization data collected for **1-Dy** through **4-Dy**, showing magnetic hysteresis. Sweep rates of 82(2) and 24(1) Oe/s were used for $|H| > 10$ kOe and $|H_{dc}| < 10$ kOe, respectively.

93 s for **3-Dy** and **4-Dy**, respectively, and fits to the 500-Oe data yielded τ_{tunnel} = 34 000 and 35 000 s, respectively. Raman relaxation parameters extracted from fits to the solution phase data under an applied field are similar for **3-Dy** and **4-Dy** (Tables S18 and S19). Overall, these results demonstrate that through-barrier relaxation processes in **3-Dy** and **4-Dy** occur at similar rates at low temperatures.

Magnetic Hysteresis. Variable-field magnetization data were collected for **1-Dy** through **4-Dy** between ±35 kOe, using a sweep rate of 82(2) Oe/s for $|H| > 10$ kOe and 24(1) Oe/s for $|H| < 10$ kOe. All compounds exhibit magnetic hysteresis, and the loops for **1-Dy** through **4-Dy** are open at zero field to temperatures as high as 4.0, 5.0, 6.5, and 7.0 K, respectively (Figure 6). For comparison, hysteresis loops are open at zero field up to 6.5 K in $[(Cp^*_2Dy)_2(\mu\text{-bpym})](BPh_4)$ for data collected with a comparable sweep rate.[47] Interestingly, the increase in the maximum hysteresis temperature upon moving from **1-Dy** to **4-Dy** is consistent with the increase in $|J_{Gd-rad}|$, where NMe_2 < OEt < Me = H < F. This result can be understood by considering that the magnetic relaxation at the maximum hysteresis temperature for each complex is dominated by an Orbach mechanism (Figures S78, S80, S81, and S83). The value of J_{Gd-rad} dictates the magnitude of U_{eff} in this series, which in turn determines the maximum temperature at which the hysteresis loop remains open.

The coercive field (H_c) can be employed to compare the rate of magnetic relaxation in a series of complexes if data are collected at comparable sweep rates. As such, the value of H_c provides an estimate of the rate of through-barrier relaxation processes in **1-Dy** through **4-Dy** at low temperatures, where Raman relaxation and quantum tunnelling of the magnetization dominate. Values of H_c = 40, 430, 760, and 580 Oe were determined for **1-Dy** through **4-Dy**, respectively, at 2 K. For comparison, H_c = 600 Oe for $[(Cp^*_2Dy)_2(\mu\text{-bpym})](BPh_4)$ at 2 K.[47] Generally, these results demonstrate that complexes with stronger exchange coupling display slower through-barrier relaxation (e.g., H_c for **3-Dy** and **4-Dy** $\gg H_c$ for **1-Dy**). However, this correlation is not strictly linear. For instance, $|J_{Gd-rad}|$ decreases by a factor of 2 from **2-Dy** to **1-Dy**, while H_c decreases by over an order of magnitude. In addition, $|J_{Gd-rad}|$ follows the trend EtO (**2-Dy**) < Me (**3-Dy**) < H < F (**4-Dy**), while H_c at 2 K follows the trend EtO < F < H < Me for both solid-state and solution samples of **3-Dy** and **4-Dy** (see section S5.6 of the Supporting Information). This result is intriguing, given that CASSCF calculations predict higher single-ion anisotropy for **4-Dy** than **3-Dy** and that both complexes are crystallographically centrosymmetric, which results in a parallel arrangement of the anisotropy axes of the Dy^{3+} ions. This result may indicate the influence of other factors on the rate of through-barrier magnetic relaxation in these complexes, and additional investigations into this behavior is ongoing.

Magnetic Relaxation in Terbium Derivatives. The compounds $[(Cp^*_2Tb)_2(\mu\text{-}5,5'\text{-}R_2bpym)](BPh_4)$ (R = NMe_2 (**1-Tb**), F (**4-Tb**)) were also synthesized in order to examine the impact of changing the lanthanide ion on single-molecule magnet behavior (see section S1 of the Supporting Information). Similar to the results for the Gd and Dy compounds, $\chi_M T$ versus T data collected for **1-Tb** and **4-Tb** under a 10 kOe field (Figure S42 and S49) pass through shallow minima at 80 and 170 K upon cooling from 300 K before rising to maximum $\chi_M T$ values of 22.7 and 27.2 emu K/mol, respectively. This behavior is again indicative of strong antiferromagnetic exchange. Moreover, the relative temperature and magnitude of the $\chi_M T$ maximum for **1-Tb** versus **4-Tb** is similar to what is observed for the corresponding Gd derivatives, implying that $|J_{Tb-rad}|$ is larger in **4-Tb** than in **1-Tb**.

Dynamic magnetic susceptibility data were also obtained for **1-Tb** and **4-Tb** (Figures S52 and S60). For **4-Tb**, relaxation times extracted from these data were fit to the equation $\tau^{-1} = \tau_0^{-1} \exp(U_{eff}/k_BT) + CT^n + \tau_{tunnel}^{-1}$ (Figure S85), yielding U_{eff} = 82 cm^{-1}, $C = 2.5 \times 10^{-2}$, n = 2.0, and $\tau_{tunnel} = 7.0 \times 10^{-1}$ s. For comparison, U_{eff} = 44 cm^{-1} for $[(Cp^*_2Tb)_2(\mu\text{-bpym})](BPh_4)$.[47] The data for **1-Tb** exhibit no temperature dependence (Figure S79) and were used to extract $\tau_{tunnel} = 2.9 \times 10^{-3}$ s. In contrast to the data for **1-Dy** through **4-Dy**, a plot of U_{eff} for **1-Tb**, **4-Tb**, and previously reported radical-containing terbium complexes versus $|J_{Gd-rad}|$ of the corresponding Gd complex is not linear (Figure S86 and Table S21). This result suggests that **1-Tb** and **4-Tb** possess low single-ion anisotropy and deviate from an Ising exchange model, thus U_{eff} is not predicted to be directly proportional to J_{Tb-rad}. Indeed, both **1-Tb** and **4-Tb** show fast quantum tunneling of the magnetization (τ_{tunnel}< 1 s) and magnetic hysteresis loops that are closed at zero field at 2 K, consistent with low single-ion anisotropy (Figures S88 and S96). The lower U_{eff} value for $[Cp^*_2Tb](BPh_4)$ relative to $[Cp^*_2Dy](BPh_4)$ further supports this assertion.[76] This analysis suggests that the lower U_{eff} values observed for organic radical-bridged terbium(III) compounds relative to their dysprosium(III) counterparts arises from lower single-ion anisotropy, rather than weaker exchange coupling interactions as has been previously proposed.[47] Modification of the ancillary Cp* ligands to increase axiality or utilization of a radical bridging ligand with weaker equatorial interactions thus represents a clear step toward increasing the magnitude of U_{eff} and the temperature at which hysteresis is observed for related terbium radical-bridged complexes. Future study of a series of

https://dx.doi.org/10.1021/jacs.0c10612
J. Am. Chem. Soc. XXXX, XXX, XXX−XXX

high-anisotropy radical-bridged terbium(III) complexes could furnish useful empirical correlations, such as the one derived here for **1-Dy** through **4-Dy**.

CONCLUSIONS

The foregoing analysis demonstrates that modifying the radical ligand substituent in the compounds $[(Cp^*_2Ln)_2(\mu\text{-}5,5'\text{-}R_2bpym)](BPh_4)$ (R = NMe_2 (**1**), OEt (**2**), Me (**3**), and F (**4**); Ln = Gd and Dy) induces drastic changes in both intramolecular magnetic exchange interactions and single-molecule magnet behavior. Electron-donating and -withdrawing substituents decrease and increase the magnitude of the exchange coupling constant, $|J_{Gd-rad}|$, respectively. Although the magnetic exchange coupling in **1-Dy** through **4-Dy** was not quantified in this study, dc magnetic susceptibility data indicate that the relative magnitudes can be correlated with $|J_{Gd-rad}|$ for the Gd^{3+} congeners. Further, we identify a linear relationship between the thermal barriers to magnetic relaxation (U_{eff}) of the highly anisotropic **1-Dy** through **4-Dy** and the $|J_{Gd-rad}|$ values for the corresponding Gd^{3+} complexes. In the case of **1-Dy** through **4-Dy**, larger $|J_{Gd-rad}|$ values are correlated with larger U_{eff} values, higher maximum hysteresis temperatures, and smaller values of τ for through-barrier relaxation processes, results that are supported by ab initio calculations. Notably, the empirical correlation between U_{eff} and $|J_{Gd-rad}|$ as shown here for **1-Dy** through **4-Dy** extends to other organic radical-bridged dysprosium compounds in the literature and suggests clear design strategies to increase U_{eff} for molecules in this class. Together, these results demonstrate the utility of systematic analysis of related compounds in developing greater predictability in the design of radical-bridged single-molecule magnets.

EXPERIMENTAL SECTION

Materials and Methods. Unless otherwise mentioned, commercial reagents were purchased from Sigma-Aldrich, Fischer, Acros, Oakwood, Strem or Alfa Aesar and used without further purification. Tetrahydrofuran (THF), hexanes, 1,2-difluorobenzene (DFB), toluene, and *N*,*N*-dimethylformamide (DMF) were sparged with argon and then dried by passing through alumina columns in a Glass Contour solvent purification system from JC Meyer. iPr$_2$NH was distilled and then dried over activated 4 Å molecular sieves. The compounds 5,5′-dimethylbipyrimidine,[35] $[Cp^*_2Gd](BPh_4)$,[77] and $[Cp^*_2Dy](BPh_4)$[47] were prepared according to literature reports. 5-Ethoxy-2-chloropyrimidine[78] and 5-(*N*,*N*-dimethyl)amino-2-chloropyrimidine[79] were previously reported in the literature but were prepared via alternative routes. All reactions were carried out in flame-dried glassware under an argon atmosphere using standard Schlenk techniques or in a nitrogen atmosphere glovebox. Compositional C, H, and N analyses were performed by the Microanalytical Facility at the University of California, Berkeley using a PerkinElmer 2400 Series II combustion analyzer.

Synthesis of 5-(*N*,*N*-Dimethyl)amino-2-chloropyrimidine. The molecule 5-amino-2-chloropyrimidine (4.5 g, 35 mmol) was dissolved in 90% formic acid (7.3 mL, 30 equiv) and to this solution was added an aqueous solution of formaldehyde (36% formaldehyde in water, 7.8 mL, 18 equiv). The reaction was heated to reflux (~105 °C) for 12 h at which time the solution was allowed to cool to 50 °C, and the solvent was removed under reduced pressure (~200 mTorr). The remaining waxy black solid was triturated with a saturated aqueous solution of sodium bicarbonate (200 mL), and the resulting brown solids were collected via vacuum filtration and purified by sublimation (~80 °C, 200 mTorr). The product was obtained as a colorless solid in 30% yield (1.65 g, 10.5 mmol).

Synthesis of 5-Ethoxy-2-chloropyrimidine. The molecule 5-hydroxy-2-chloropyrimidine (1.0 g, 7.7 mmol) was dissolved in DMF (15 mL) and to this solution was added potassium carbonate (1.6 g, 12 mmol, 1.5 equiv). Subsequently, iodoethane (0.92 mL, 1.8 g, 12 mmol, 1.5 equiv) was added dropwise. The reaction was stirred at 25 °C for 1 h, at which time water (50 mL) was added. The resulting mixture was extracted with EtOAc (3 × 30 mL) and the organic layers were combined, dried over Na_2SO_4, and concentrated to yield a light brown solid. This solid was dissolved in 25% EtOAc in hexanes and purified via filtration over silica gel. The product was obtained as a colorless solid in 86% yield (1.05 g, 6.62 mmol).

Synthesis of 5,5′-Di-(*N*,*N*-dimethylamino)-2,2′-bipyrimidine ($(NMe_2)_2$bpym). Analogous to a literature synthesis of 2,2′-bipyrimidine,[38] nickel(II) chloride hexahydrate (360 mg, 1.5 mmol, 0.25 equiv) and triphenylphosphine (1.6 g, 6.0 mmol, 1.0 equiv) were placed in a Schlenk flask and dried under reduced pressure (~200 mTorr) for 20 min. The solids were subsequently dissolved in dry, degassed DMF (30 mL) under argon with vigorous stirring, and to this solution was added Zn powder (200 mg, 3.0 mmol, 0.5 equiv). The resulting green solution became deep red in color and was stirred for 1 h at 25 °C, at which point 5-(*N*,*N*-dimethyl)amino-2-chloropyrimidine (950 mg, 6.0 mmol) was added. The solution became black in color and was stirred for 1 h at 25 °C, followed by 48 h at 50 °C. The black solution was cooled to room temperature and filtered through diatomaceous earth, and the filter cake was washed with DMF (30 mL). The filtrate was concentrated under reduced pressure (~50 °C, 200 mTorr) to yield a brown oil, to which was added a solution of ethylenediaminetetraacetic acid (2.6 g, 9.0 mmol, 1.5 equiv) in aqueous ammonia (7% NH_3 in water; 20 mL). This solution was stirred for 3 h, becoming blue in color and precipitating colorless solids that were collected via vacuum filtration. The solids were triturated in Et_2O (3 × 20 mL) to remove triphenylphosphine and were then purified via recrystallization (1:10 $CHCl_3$/hexanes or MeOH). The product was obtained as a pale yellow solid in 33% yield (480 mg, 2.0 mmol). ^{1}H NMR (600 MHz, $CDCl_3$) δ = 8.40 (s, 4H), 3.10 (s, 12H) ppm. ^{13}C NMR (150 MHz, $CDCl_3$) δ = 150.0, 142.5, 140.4, 39.7 ppm. HRMS (ESI+) m/z calcd. for $C_{12}H_{17}N_6$ $[M+H^+]$: 245.1509; found: 245.1511.

Synthesis of 5,5′-Diethoxy-2,2′-bipyrimidine ($(OEt)_2$bpym). Analogous to the synthesis of $(NMe_2)_2$bpym, nickel(II) chloride hexahydrate (380 mg, 1.6 mmol, 0.25 equiv) and triphenylphosphine (1.7 g, 6.4 mmol, 1 equiv) were placed in a Schlenk flask and dried under reduced pressure (~200 mTorr) for 20 min. The solids were subsequently dissolved in dry, degassed DMF (40 mL) under argon with vigorous stirring, and to this solution was added Zn powder (210 mg, 3.2 mmol, 0.5 equiv). The resulting green solution became deep red in color and was stirred for 1h at 25 °C, at which point 5-ethoxy-2-chloropyrimidine (1.0 g, 6.4 mmol) was added. The solution became black in color and was stirred for 1 h at 25 °C, followed by 48 h at 50 °C. The black solution was cooled to room temperature, filtered through diatomaceous earth, and the filter cake was washed with DMF (40 mL). The filtrate was concentrated under reduced pressure (~50 °C, 200 mTorr) to yield a brown oil to which was added a solution of ethylenediaminetetraacetic acid (2.7 g, 9.6 mmol, 1.5 equiv) in aqueous ammonia (7% NH_3 in water; 30 mL). This solution was stirred for 3 h, becoming green in color, and it was subsequently extracted with $CHCl_3$ (3 × 30 mL). The organic layers were combined, dried over Na_2SO_4, and concentrated. The resulting solids were triturated in Et_2O (3 × 30 mL) to remove excess triphenylphosphine and then purified via recrystallization (1:10 $CHCl_3$/hexanes or MeOH). The product was obtained as a colorless solid in 37% yield (580 mg, 2.4 mmol). ^{1}H NMR (500 MHz, $CDCl_3$) δ = 8.55 (s, 4H), 4.20 (q, J = 7.0 Hz, 4H), 1.46 (t, J = 7.0 Hz, 6H) ppm. ^{13}C NMR (125 MHz, $CDCl_3$) δ = 154.8, 152.7, 144.3, 64.8, 14.7 ppm. HRMS (ESI+) m/z calcd. for $C_{12}H_{15}O_2N_4$ $[M+H^+]$: 247.1190; found: 247.1191.

Synthesis of 5-Fluoro-2-tributylstannylpyrimidine. A solution of iPr$_2$NH (0.78 mL, 5.5 mmol, 1.3 equiv) in dry THF (10 mL) was stirred at 0 °C in a Schlenk flask under argon. To this solution was added n-BuLi (2.5 M in hexanes, 2.0 mL, 5.0 mmol, 1.2 equiv) dropwise, and the resulting pale yellow solution was stirred for 30 min at 0 °C. $HSnBu_3$ (1.3 mL, 4.8 mmol, 1.1 equiv) was then added

https://dx.doi.org/10.1021/jacs.0c10612
J. Am. Chem. Soc. XXXX, XXX, XXX−XXX

dropwise, and the light green solution was stirred for 10 min at 0 °C, cooled to −78 °C for 5 min, and then transferred via cannula to a solution of 5-fluoro-2-chloropyrimidine (580 mg, 0.40 mL, 4.4 mmol) in dry THF (20 mL) that had been precooled to −78 °C. The resulting deep orange-red solution was stirred at −78 °C for 2 h and then 0 °C for 2 h, at which point it was quenched by addition of H_2O (30 mL). The reaction mixture was extracted with EtOAc (3 × 30 mL), and the organic layers were dried over Na_2SO_4 and then concentrated under reduced pressure to yield a brown oil, which was purified via column chromatography on silica gel (R_f = 0.70, 10% EtOAc in hexanes). The product was obtained as a colorless oil in 35% yield (590 mg, 1.5 mmol). ^{1}H NMR (400 MHz, C_6D_6) δ = 8.14 (s, 2H), 1.72 (m, 6H), 1.40 (m, 6H), 1.29 (t, J = 7.3 Hz, 6H), 0.92 (t, J = 7.3 Hz, 9H) ppm. ^{13}C NMR (150 MHz, C_6D_6) δ = 184.2 (d, J = 10.7 Hz), 157.7 (d, J = 266.7 Hz), 142.6 (d, J = 15.3 Hz), 29.4, 27.7, 14.0, 10.9 ppm. ^{19}F-NMR (376 MHz, C_6D_6) −136.7 ppm. HRMS (ESI+) m/z calcd. for $C_{16}H_{30}N_2FSn$ [M+H$^+$]: 389.1410; found: 389.1410.

Synthesis of 5-Trifluoromethyl-2-tributylstannylpyrimidine. Analogous to the synthesis of 5-fluoro-2-tributylstannylpyrimidine, a solution of iPr$_2$NH (0.58 mL, 4.1 mmol, 1.3 equiv) in dry THF (10 mL) was stirred at 0 °C in a Schlenk flask under argon. To this solution was added n-BuLi (2.5 M in hexanes, 1.5 mL, 3.8 mmol, 1.2 equiv) dropwise, and the resulting solution was stirred for 30 min at 0 °C. $HSnBu_3$ (1.0 mL, 3.7 mmol, 1.1 equiv) was then added dropwise and the solution was stirred for 10 min at 0 °C, cooled to −78 °C for 5 min, and then transferred via cannula to a solution of 5-trifluoromethyl-2-chloropyrimidine (600 mg, 3.3 mmol) in dry THF (20 mL) that had been precooled to −78 °C. The resulting solution was stirred at −78 °C for 2 h and then 0 °C for 2 h, at which point it was quenched by addition of H_2O (30 mL). The reaction mixture was extracted with EtOAc (3 × 30 mL), and the organic layers were dried over Na_2SO_4 and concentrated under reduced pressure to yield a brown oil, which was purified via column chromatography on silica gel (R_f = 0.60, 10% EtOAc in hexanes). The product was obtained as a colorless oil in 50% yield (720 mg, 1.6 mmol). ^{1}H NMR (600 MHz, C_6D_6) δ = 8.38 (s, 2H), 1.33 (m, 6H), 1.14 (m, 6H), 0.82 (m, 15H) ppm. ^{13}C NMR (150 MHz, C_6D_6) δ = 162.4, 155.4 (t, J = 7.6 Hz), 134.2 (q, J = 14.3 Hz), 133.2 (q, J = 289.7 Hz), 28.9, 27.5, 13.8, 10.4 ppm. ^{19}F-NMR (376 MHz, C_6D_6) −98.4 ppm. HRMS (ESI+) m/z calcd. for $C_{17}H_{30}N_2F_3Sn$ [M+H$^+$]: 439.1378; found: 439.1384.

Synthesis of 5,5′-Difluoro-2,2′-bipyrimidine (F_2bpym). The molecules 5-fluoro-2-chloropyrimidine (130 mg, 1.0 mmol), 5-fluoro-2-tributylstannylpyrimidine (370 mg, 1.0 mmol, 1.0 equiv), copper(I) chloride (87 mg, 1.1 mmol, 1.1 equiv), and Pd(dppf)Cl$_2$ (70 mg, 0.1 mmol, 10 mol %) were dissolved in dry THF (10 mL) in a Schlenk flask under argon. The resulting solution was heated to 70 °C for 18 h, first turning yellow and then brown. The reaction was then allowed to cool to ambient temperature, concentrated under reduced pressure, and a solution of ethylenediaminetetraacetic acid (0.43 g, 1.5 mmol, 1.5 equiv) in aqueous ammonia (7% NH_3 in water; 20 mL) was added. This solution was stirred for 3 h, becoming green in color, and then was extracted with Et_2O (3 × 20 mL) and subsequently with CH_2Cl_2 (3 × 20 mL). The CH_2Cl_2 layers were combined, dried over Na_2SO_4, and concentrated under reduced pressure to yield a brown solid that was purified via sublimation (∼120 °C, 200 mTorr). The product was obtained as a colorless solid in 57% yield (106 mg, 0.6 mmol). ^{1}H NMR (500 MHz, $CDCl_3$) δ = 8.86 (s, 4H) ppm. ^{13}C NMR (125 MHz, $CDCl_3$) δ = ppm. ^{19}F-NMR (376 MHz, $CDCl_3$) −134.1 ppm. HRMS (ESI+) m/z calcd. for $C_8H_5N_4F_2$ [M+H$^+$]: 195.0477; found: 195.0479.

Synthesis of 5-Fluoro-5′-trifluoromethyl-2,2′-bipyrimidine (F-CF_3-bpym). Analogous to the synthesis of F_2bpym, 5-trifluoromethyl-2-chloropyrimidine (280 mg, 1.6 mmol, 1.5 equiv), 5-fluoro-2-tributylstannylpyrimidine (400 mg, 1.1 mmol), copper(I) chloride (110 mg, 1.2 mmol, 1.1 equiv), and Pd(dppf)Cl$_2$ (76 mg, 0.1 mmol, 10 mol %) were dissolved in dry THF (10 mL) in a Schlenk flask under argon. The resulting solution was heated to 70 °C for 18 h, first turning yellow and then brown. The reaction was then allowed to cool to ambient temperature, concentrated under reduced pressure, and a solution of ethylenediaminetetraacetic acid (0.47 g, 1.6 mmol, 1.5 equiv) in aqueous ammonia (7% NH_3 in water; 20 mL) was added. This solution was stirred for 3 h, becoming green in color, and then was extracted with hexanes (3 × 20 mL) and subsequently with CH_2Cl_2 (3 × 20 mL). The CH_2Cl_2 layers were combined, dried over Na_2SO_4, and concentrated to yield a brown solid that was purified via sublimation (∼120 °C, 200 mTorr). The product was obtained as a colorless solid in 46% yield (102 mg, 0.5 mmol). ^{1}H NMR (500 MHz, $CDCl_3$) δ = 9.22 (s, 2H), 8.88 (s, 2H) ppm. ^{13}C NMR (125 MHz, $CDCl_3$) δ = 163.8, 158.2 (d, J = 270.0 Hz), 157.4, 155.6 (q, J = 3.3 Hz), 146.3 (d, J = 20.7 Hz), 125.0 (q, J = 34.0 Hz), 122.6 (q, J = 271.0 Hz) ppm. ^{19}F-NMR (376 MHz, $CDCl_3$) −61.5, −132.3 ppm. HRMS (ESI+) m/z calcd. for $C_9H_5N_4F_4$ [M+H$^+$]: 245.0445; found: 245.0446.

Synthesis of [(GdCp*$_2$)$_2$(μ-5,5′-(NMe$_2$)$_2$bpym)](BPh$_4$) (1-Gd). The molecule [Cp*$_2$Gd](BPh$_4$) (42.5 mg, 0.0568 mmol) was suspended in toluene (4 mL), and to this slurry was added (NMe$_2$)$_2$bpym (6.9 mg, 0.028 mmol, 0.5 equiv). The resulting solution was stirred for 30 min, during which time it changed color from pale yellow to bright orange. At this point, KC_8 (3.8 mg, 0.028 mmol, 0.5 equiv) was added in THF (0.5 mL), and the reaction became dark brown in color. After stirring 30 min, the solvent was removed under reduced pressure and THF (2 mL) was added to form a dark reddish-black solution. Black and white insoluble solids were removed by filtration through diatomaceous earth, and then the solution was layered with toluene (2 mL) and cooled to −30 °C, affording red, block-shaped crystals of **1-Gd** after 48 h (22.0 mg, 55% yield). Anal. Calcd. For $C_{76}H_{96}BN_6Gd_2$: C, 64.33; H, 6.82; N, 5.92. Found: C, 64.54; H, 6.78; N, 5.92.

Synthesis of [(GdCp*$_2$)$_2$(μ-5,5′-(OEt)$_2$bpym)](BPh$_4$) (2-Gd). Analogous to the synthesis of **1-Gd**, [Cp*$_2$Gd](BPh$_4$) (42.5 mg, 0.0568 mmol) was stirred in toluene (4 mL) with (OEt)$_2$bpym (7.0 mg, 0.028 mmol, 0.5 equiv) and then subsequently KC_8 (3.8 mg, 0.028 mmol, 0.5 equiv) was added in THF (0.5 mL). Insoluble solids were removed by centrifugation and then red, block-shaped crystals of **2-Gd** were grown from a layered THF-toluene solution (2 mL THF, 2 mL toluene) cooled to −30 °C for 48 h (15.6 mg, 39% yield). Anal. Calcd. For $C_{76}H_{94}BN_4O_2Gd_2$: C, 64.24; H, 6.67; N, 3.94. Found: C, 64.55; H, 6.43; N, 4.32.

Synthesis of [(GdCp*$_2$)$_2$(μ-5,5′-Me$_2$bpym)](BPh$_4$) (3-Gd). Analogous to the synthesis of **1-Gd**, [Cp*$_2$Gd](BPh$_4$) (42.5 mg, 0.0568 mmol) was stirred in toluene (4 mL) with Me$_2$bpym (5.3 mg, 0.028 mmol, 0.5 equiv) and then subsequently KC_8 (3.8 mg, 0.028 mmol, 0.5 equiv) was added in THF (0.5 mL). Insoluble solids were removed by centrifugation and then red, block-shaped crystals of **3-Gd** were grown from a layered THF-toluene solution (2 mL THF, 2 mL toluene) cooled to −30 °C for 48 h (14.0 mg, 36% yield). Anal. Calcd. for $C_{74}H_{90}BN_4Gd_2$: C, 65.31; H, 6.67; N, 4.12. Found: C, 65.21; H, 6.68; N, 3.86.

Synthesis of [(GdCp*$_2$)$_2$(μ-5,5′-F$_2$bpym)](BPh$_4$) (4-Gd). The molecule[Cp*$_2$Gd](BPh$_4$) (77.0 mg, 0.103 mmol) was suspended in toluene (4 mL) and to this slurry was added F_2bpym (10.0 mg, 0.0515 mmol, 0.5 equiv). This reddish-orange solution was stirred for 30 min and then KC_8 (6.9 mg, 0.052 mmol, 0.5 equiv) was added in toluene (0.5 mL). The resulting reddish-black solution was stirred for 24 h and then concentrated under reduced pressure, dissolved in 1,2-difluorobenzene (DFB, 2 mL), and filtered through diatomaceous earth. Red, block-shaped crystals of **4-Gd** were grown from a layered DFB-hexanes solution (2 mL DFB, 2 mL hexanes) stored at 25 °C for 48 h (30.6 mg, 43% yield). Anal. Calcd. For $C_{76}H_{96}BN_6Dy_2$: C, 63.18; H, 6.19; N, 4.00. Found: C, 63.08; H, 6.18; N, 3.79.

Mass Spectrometry. High-res mass spectrometric data were obtained from the Mass Spectrometry Facility at the University of California, Berkeley, on a Finnigan/Thermo LTQ-FT instrument (ESI); data acquisition and processing were performed using the Xcalibur software.

NMR Spectroscopy. NMR spectroscopic data were obtained for solutions in deuterated solvents ($CDCl_3$ or C_6D_6) purchased from Cambridge Isotope Laboratories, Inc. ^{1}H NMR, ^{13}C NMR, and ^{19}F NMR data were recorded on Bruker AVQ-400, DRX-500, AV-500,

https://dx.doi.org/10.1021/jacs.0c10612
J. Am. Chem. Soc. XXXX, XXX, XXX−XXX

and AV-600 spectrometers. Chemical shifts (δ) are reported in ppm relative to the residual solvent peak (δ 7.26 for $CDCl_3$ and δ 7.16 for C_6D_6 for ^{1}H NMR; δ 77.16 for $CDCl_3$ and δ 128.06 for C_6D_6 for ^{13}C NMR). Data for ^{1}H NMR are reported in the following format: chemical shift (ppm) (multiplicity (s = singlet, d = doublet, t = triplet, q = quartet, m = multiplet), coupling constant (Hz), integration). Data for ^{13}C NMR and ^{19}F-NMR are reported in terms of chemical shift (ppm) with coupling constants for ^{19}F−^{13}C coupling where applicable.

Infrared Spectroscopy. FT-IR spectra were recorded on a PerkinElmer Avatar Spectrum 400 FTIR Spectrometer equipped with attenuated total reflectance (ATR).

Single-Crystal X-ray Diffraction. Single-crystal X-ray diffraction data were collected at small-molecule crystallography beamlines (beamline 11.3.1 for 2-Gd, 3-Gd, and 3-Dy; and beamline 12.2.1 for **2-Dy**, **4-Gd**, and **4-Dy**) at the Advanced Light Source, Lawrence Berkeley National Laboratory. Single crystals were coated with Paratone-N oil, mounted on a MiTeGen loop, and frozen at 100 K under a stream of N_2 from an Oxford Cryostems Cryostream 700 Plus on a Bruker AXS D8 diffractometer. Data were collected through a combination of 4° and 1° ϕ and ω scans. Data reduction was performed through SAINT and absorption correction through SADABS (or TWINABS for 3-Dy).[80−82]

Single-crystal X-ray diffraction data for **1-Dy** were collected at the University of California, Berkeley using a Rigaku XtaLAB p200 equipped with a MicroMax-007 HF microfocus rotating anode and a Pilatus 200 K hybrid pixel array detector at 100 K under a N_2 stream of an Oxford Cryostems Cryostream with Mo Kα radiation (graphite monochromator). The frames were integrated with CrysAlis^{Pro} software, including a multiscan absorption correction that was applied using the SCALE3 ABSPACK scaling algorithm within CrysAlis^{Pro}.[83]

Structure solutions were performed by SHELXT[84] using direct methods and were refined by least-squares refinement against F^2 by SHELXL[85] following standard procedures via OLEX2 crystallographic software.[86] For all structures, all non-hydrogen atoms were refined anisotropically. All hydrogen atoms were placed on geometrically calculated positions using the riding model and refined isotropically.

Magnetic Measurements. Each sample for magnetic measurements was prepared by adding a polycrystalline powder (20.9 mg of 1-Gd, 13.6 mg of 1-Dy, 7.0 mg of 1-Tb, 7.0 mg of 2-Gd, 17.4 mg of 2-Dy, 6.8 mg of 3-Gd, 16.2 mg of 3-Dy, 4.6 mg of 4-Gd, 10.6 mg of 4-Dy, and 12.4 mg of 4-Tb) to a 5 mm i.d./7 mm o.d. quartz tube with a raised quartz platform. A layer of eicosane was added on top of the sample (14.5 mg for 1-Gd, 16.7 mg for 1-Dy, 15.0 mg for 1-Tb, 15.7 mg for 2-Gd, 17.7 mg for 2-Dy, 18.1 mg for 3-Gd, 28.8 mg for 3-Dy, 16.6 mg for 4-Gd, 18.7 mg for 4-Dy, and 18.9 mg for 4-Tb) to provide good thermal contact between the sample and the bath and to prevent crystallite torqueing. The tubes were fitted with Teflon-sealable adapters, evacuated using a glovebox vacuum pump, and then flame-sealed with an O_2/H_2 flame under vacuum. After flame-sealing, the eicosane was melted in a 45 °C water bath. Magnetic measurements were also conducted on a 7.8 mM solution of 3-Dy and an 8.0 mM solution of 4-Dy in 1,2-difluorobenzene.

Magnetic susceptibility measurements were collected using a Quantum Design MPMS2 SQUID magnetometer. All data were corrected for diamagnetic contributions from the core diamagnetism of the sample and for the diamagnetism of the eicosane used to suspend the sample, estimated using Pascal's constants to give corrections of χ_{dia} = −0.000814 for **1-Gd**, −0.000812 for **1-Dy**, −0.000812 for **1-Tb**, −0.000806 for **2-Gd**, −0.000869 for **2-Dy**, −0.000773 for **3-Gd**, −0.000771 for **3-Dy**, −0.000756 for **4-Gd**, −0.000754 for **4-Dy**, and −0.000754 for **4-Tb**.

Fits to the dc susceptibility data for **1-Gd** through **4-Gd** were performed using PHI.[87] Uncertainties for values of τ and magnetic relaxation parameters were determined using the α and n values extracted from fits to ac susceptibility and dc relaxation measurements, respectively.[88,89]

Calculations. The local electronic and magnetic properties of the Dy^{3+} ions in 1-Dy through 4-Dy and $[(Cp^*_2Dy)_2(\mu\text{-ind})]^-$ were calculated with the MOLCAS 8.2 program.[90] Fragment calculations were performed on the single crystal X-ray diffraction structures with nearby Dy^{3+} ions replaced with Lu^{3+}. The methyl groups of the cyclopentadienyl ligand around each Lu^{3+} ion were replaced by hydrogen atoms. The Cholesky decomposition threshold was set to 5×10^{-8} Hartree to save disk space. The ANO-RCC basis set was used for all atoms (Table S22). Four point charges on the bridging carbon and nitrogen atoms, each −0.25e, were included to consider the electrostatic potential from the unpaired electron of $bpym^{\bullet-}$. CASSCF calculations comprised seven 4f type orbitals. Twenty-one sextet, 128 quartet and 130 doublet states were admixed by spin−orbit coupling within the RASSI program. Based on the obtained spin−orbital states, local magnetic properties were calculated within the SINGLE_ANISO program.[91] Finally, the exchange interaction was included within the POLY_ANISO module.[92,93]

To estimate the exchange coupling parameters between the Dy^{3+} ions and the bpym-radical ligand, broken-symmetry DFT calculations[94] were employed by using ORCA 3.0.0[95] with SVP basis set, B3LYP functional, Grid6 and TightSCF settings. Because Dy^{3+} ions are multiconfigurational in their nature, they cannot be treated adequately by DFT methods. Therefore, the Dy^{3+} ions were replaced with Gd^{3+}, while preserving the position of all atoms intact. In this way one can extract the exchange interaction between the Gd^{3+} ions and the radical and then rescale it to the spin of Dy^{3+} to calculate J_{Dy-rad}. This is achieved by multiplying the former value by 49/25.[71]

■ ASSOCIATED CONTENT

Supporting Information

The Supporting Information is available free of charge at https://pubs.acs.org/doi/10.1021/jacs.0c10612.

Additional experimental details, NMR spectroscopy, IR spectroscopy, X-ray crystallography refinement details, magnetic measurements, description of calculations, and supplementary discussion (PDF)

Crystallographic structure data for **3-Dy** (CIF)

Crystallographic structure data for **2-Gd** (CIF)

Crystallographic structure data for **2-Dy** (CIF)

Crystallographic structure data for **4-Dy** (CIF)

Crystallographic structure data for **4-Gd** (CIF)

Crystallographic structure data for **1-Dy** (CIF)

Crystallographic structure data for **3-Gd** (CIF)

■ AUTHOR INFORMATION

Corresponding Author

Jeffrey R. Long − *Department of Chemistry and Department of Chemical and Biomolecular Engineering, University of California, Berkeley, Berkeley, California 94720, United States; Materials Sciences Division, Lawrence Berkeley National Laboratory, Berkeley, California 94720, United States;* orcid.org/0000-0002-5324-1321; Email: jrlong@berkeley.edu

Authors

Colin A. Gould − *Department of Chemistry, University of California, Berkeley, Berkeley, California 94720, United States;* orcid.org/0000-0001-9539-1582

Edward Mu − *Department of Chemistry, University of California, Berkeley, Berkeley, California 94720, United States*

Veacheslav Vieru − *Theory of Nanomaterials Group, Katholieke Universiteit Leuven, 3001 Leuven, Belgium*

Lucy E. Darago − *Department of Chemistry, University of California, Berkeley, Berkeley, California 94720, United States*

https://dx.doi.org/10.1021/jacs.0c10612
J. Am. Chem. Soc. XXXX, XXX, XXX−XXX

Khetpakorn Chakarawet − *Department of Chemistry, University of California, Berkeley, Berkeley, California 94720, United States;* orcid.org/0000-0001-5905-3578

Miguel I. Gonzalez − *Department of Chemistry, University of California, Berkeley, Berkeley, California 94720, United States*

Selvan Demir − *Department of Chemistry, University of California, Berkeley, Berkeley, California 94720, United States; Department of Chemistry, Michigan State University, East Lansing, Michigan 48824, United States*

Complete contact information is available at: https://pubs.acs.org/10.1021/jacs.0c10612

Notes

The authors declare no competing financial interest.

■ ACKNOWLEDGMENTS

This work was supported by NSF grant CHE-1800252. Single-crystal X-ray diffraction experiments were performed at beamlines 11.3.1 and 12.2.1 at the Advanced Light Source at Lawrence Berkeley National Laboratory. The Advanced Light Source is supported by the Director, Office of Science, Office of Basic Energy Sciences, of the U.S. Department of Energy under Contract No. DE-AC02-05CH11231. We thank the National Science Foundation Graduate Research Fellowship Program for support of C.A.G. and L.E.D. We thank Dr. Hasan Celik and UC Berkeley's NMR facility in the College of Chemistry (CoC-NMR) for spectroscopic assistance. Instruments in the CoC-NMR are supported in part by an NIH Grant S10OD024998. V.V. acknowledges the postdoctoral fellowship of Fonds Wetenschappelijk Onderzoek Vlaanderen (FWO, Flemish Science Foundation) and the V435018N FWO travel grant to UC Berkeley. We also thank Dr. Rebecca L. Siegelman for assistance with crystallography, Dr. T. David Harris for helpful discussions, and Dr. Katie R. Meihaus for editorial assistance.

■ REFERENCES

(1) Sessoli, R.; Gatteschi, D.; Caneschi, A.; Novak, M. A. Magnetic bistability in a metal-ion cluster. *Nature* **1993**, *365*, 141−143.

(2) Gatteschi, D.; Sessoli, R.; Villain, J. *Molecular Nanomagnets*; Oxford University Press: New York, 2006.

(3) Bogani, L.; Wernsdorfer, W. Molecular spintronics using single-molecule magnets. *Nat. Mater.* **2008**, *7*, 179−186.

(4) Vincent, R.; Klyatskaya, S.; Ruben, M.; Wernsdorfer, W.; Balestro, F. Electronic read-out of a single nuclear spin using a molecular spin transistor. *Nature* **2012**, *488*, 357−360.

(5) Thiele, S.; Balestro, F.; Ballou, R.; Klyatskaya, S.; Ruben, M.; Wernsdorfer, W. Electrically driven nuclear spin resonance in single-molecule magnets. *Science* **2014**, *344*, 1135−1138.

(6) Heersche, H. B.; de Groot, Z.; Folk, J. A.; van der Zant, H. S. J.; Romeike, C.; Wegewijs, M. R.; Zobbi, L.; Barreca, D.; Tondello, E.; Cornia, A. Electron Transport through Single Mn12 Molecular Magnets. *Phys. Rev. Lett.* **2006**, *96*, 206801.

(7) Liddle, S. T.; van Slageren, J. Improving f-element single molecule magnets. *Chem. Soc. Rev.* **2015**, *44*, 6655−6669.

(8) Escalera-Moreno, L.; Baldovi, J. J.; Gaita-Arino, A.; Coronado, E. Spin states, vibrations, and spin relaxation in molecular nanomagnets and spin qubits: a critical perspective. *Chem. Sci.* **2018**, *9*, 3265−3275.

(9) Woodruff, D. N.; Winpenny, R. E. P.; Layfield, R. A. Lanthanide Single-Molecule Magnets. *Chem. Rev.* **2013**, *113*, 5110−5148.

(10) Lu, J.; Guo, M.; Tang, J. Recent Developments in Lanthanide Single-Molecule Magnets. *Chem. - Asian J.* **2017**, *12*, 2772−2779.

(11) Rinehart, J. D.; Long, J. R. Exploiting Single-Ion Anisotropy in the Design of f-Element Single-Molecule Magnets. *Chem. Sci.* **2011**, *2*, 2078−2085.

(12) Chilton, N. F.; Collison, D.; McInnes, E. J. L.; Winpenny, R. E. P.; Soncini, A. An electrostatic model for the determination of magnetic anisotropy in dysprosium complexes. *Nat. Commun.* **2013**, *4*, 2551.

(13) Sievers, J. Z. Asphericity of 4*f*-shells in their Hund's rule ground states. *Z. Phys. B: Condens. Matter Quanta* **1982**, *45*, 289−296.

(14) Ungur, L.; Chibotaru, L. F. Magnetic anisotropy in the excited states of low symmetry lanthanide complexes. *Phys. Chem. Chem. Phys.* **2011**, *13*, 20086.

(15) Chilton, N. F.; Goodwin, C. A. P.; Mills, D. P.; Winpenny, R. E. P. The first near-linear bis(amide) f-block complex: a blueprint for a high temperature single molecule magnet. *Chem. Commun.* **2015**, *51*, 101.

(16) Ding, Y.-S.; Han, T.; Zhai, Y.-Q.; Reta, D.; Chilton, N. F.; Winpenny, R. E. P.; Zheng, Y.-Z. A Study of Magnetic Relaxation in Dysprosium(III) Single-Molecule Magnets. *Chem. - Eur. J.* **2020**, *26*, 5893.

(17) Harriman, K. L.; Korobkov, I.; Murugesu, M. From a Piano Stoll to a Sandwich: A Stepwise Route for Improving the Slow Magnetic Relaxation Properties of Thulium. *Organometallics* **2017**, *36*, 4515−4518.

(18) Jiang, S.-D.; Liu, S.-S.; Zhou, L.-N.; Wang, B.-W.; Wang, Z.-M.; Gao, S. Series of Lanthanide Organometallic Single-Ion Magnets. *Inorg. Chem.* **2012**, *51*, 3079−3087.

(19) Goodwin, C. A. P.; Ortu, F.; Reta, D.; Chilton, N. F.; Mills, D. P. Molecular magnetic hysteresis at 60 K in dysprosocenium. *Nature* **2017**, *548*, 439−442.

(20) Guo, F.-S.; Day, B. M.; Chen, Y.-C.; Tong, M.-L.; Mansikkamäki, A.; Layfield, R. A. A Dysprosium Metallocene Single-Molecule Magnet Functioning at the Axial Limit. *Angew. Chem., Int. Ed.* **2017**, *56*, 11445−11449.

(21) McClain, K. R.; Gould, C. A.; Chakarawet, K.; Teat, S. J.; Groshens, T. J.; Long, J. R.; Harvey, B. G. High-temperature magnetic blocking and magneto-structural correlations in a series of dysprosium(III) metallocenium single-molecule magnets. *Chem. Sci.* **2018**, *9*, 8492−8503.

(22) Guo, F.-S.; Day, B. M.; Chen, Y.-C.; Tong, M.-L.; Mansikkamäki, A.; Layfield, R. A. Magnetic hysteresis up to 80 K in a dysprosium metallocene single-molecule magnet. *Science* **2018**, *362*, 1400−1403.

(23) Demir, S.; Gonzalez, M. I.; Darago, L. E.; Evans, W. J.; Long, J. R. Giant coercivity and high magnetic blocking temperatures for N_2^{3-} radical-bridged dilanthanide complexes upon ligand dissociation. *Nat. Commun.* **2017**, *8*, 2144.

(24) Rinehart, J. D.; Fang, M.; Evans, W. J.; Long, J. R. Strong exchange and magnetic blocking in N_2^{3-}-radical-bridged lanthanide complexes. *Nat. Chem.* **2011**, *3*, 538−542.

(25) Rinehart, J. D.; Fang, M.; Evans, W. J.; Long, J. R. A N_2^{3-} Radical-Bridged Terbium Complex Exhibiting Magnetic Hysteresis at 14 K. *J. Am. Chem. Soc.* **2011**, *133*, 14236−14239.

(26) Demir, S.; Jeon, I. R.; Long, J. R.; Harris, T. D. Radical ligand-containing single-molecule magnets. *Coord. Chem. Rev.* **2015**, *289*−*290*, 149−176.

(27) Giansiracusa, M. J.; Moreno-Pineda, E.; Hussain, R.; Marx, R.; Martinez Prada, M.; Neugebauer, P.; Al-Badran, S.; Collison, D.; Tuna, F.; van Slageren, J.; Carretta, S.; Guidi, T.; McInnes, E. J. L.; Winpenny, R. E. P.; Chilton, N. F. Measurement of Magnetic Exchange in Asymmetric Lanthanide Dimetallics: Toward a Transferable Theoretical Framework. *J. Am. Chem. Soc.* **2018**, *140*, 2504−2513.

(28) Meng, Y.-S.; Xiong, J.; Yang, M.-W.; Qiao, Y.-S.; Zhong, Z.-Q.; Sun, H.-L.; Han, J.-B.; Liu, T.; Wang, B.-W.; Gao, S. Experimental Determination of Magnetic Anisotropy in Exchange-Bias Dysprosium Metallocene Single-Molecule Magnets. *Angew. Chem., Int. Ed.* **2020**, *59*, 13037−13043.

(29) Chaudhuri, P.; Wagner, R.; Weyhermüller, T. Ferromagnetic vs Antiferromagnetic Coupling in Bis(μ-phenoxo)dicopper(II) Complexes. Tuning of the Nature of Exchange Coupling by Remote Ligand Substituents. *Inorg. Chem.* **2007**, *46*, 5134−5136.
(30) Ni, Z.-H.; Zhang, L.-F.; Tangoulis, V.; Wernsdorfer, W.; Cui, A.-L.; Sato, O.; Kou, H.-Z. Substituent Effect on Formation of Heterometallic Molecular Wheels: Synthesis, Crystal Structure, and Magnetic Properties. *Inorg. Chem.* **2007**, *46*, 6029−6037.
(31) Thompson, L. K.; Mandal, S. K.; Tandon, S. S.; Bridson, J. N.; Park, M. K. Magnetostructural Correlations in Bis(μ_2-phenoxide)-Bridged Macrocyclic Dinuclear Copper(II) Complexes. Influence of Electron-Withdrawing Substituents on Exchange Coupling. *Inorg. Chem.* **1996**, *35*, 3117−3125.
(32) Liu, X.-W.; Wu, Z.; Chen, J.-T.; Li, L.; Chen, P.; Sun, W.-B. Regulating the single-molecule magnetic properties of phenol oxygen-bridged binuclear lanthanide complexes through the electronic and spatial effect of the substituents. *Inorg. Chem. Front.* **2020**, *7*, 1229−1238.
(33) Wang, W.-M.; Qiao, W.-Z.; Zhang, H.-X.; Wang, S.-Y.; Nie, Y.-Y.; Chen, H.-M.; Liu, Z.; Gao, H.-L.; Cui, J.-Z.; Zhao, B. Structures and magnetic properties of several phenoxo-O bridged dinuclear lanthanide complexes: Dy derivatives displaying substituent dependent magnetic relaxation behavior. *Dalton Trans.* **2016**, *45*, 8182−8191.
(34) Habib, F.; Brunet, G.; Vieru, V.; Korobkov, I.; Chibotaru, L. F.; Murugesu, M. Significant Enhancement of Energy Barriers in Dinuclear Dysprosium Single-Molecule Magnets Through Electron-Withdrawing Effects. *J. Am. Chem. Soc.* **2013**, *135*, 13242−13245.
(35) Inagaki, A.; Yatsuda, S.; Edure, S.; Suzuki, A.; Takahashi, T.; Akita, M. Synthesis of Pd Complexes Combined with Photosensitizing of a Ruthenium(II) Polypyridyl Moiety through a Series of Substituted Bipyrimidine Bridges. Substituent Effect of the Bridging Ligand on the Photocatalytic Dimerization of α-Methylstyrene. *Inorg. Chem.* **2007**, *46*, 2432−2445.
(36) Murata, K.; Araki, M.; Inagaki, A.; Akita, M. Syntheses, photophysical properties, and reactivities of novel bichromophoric Pd complexes composed of Ru(II)-polypyridyl and naphthyl moieties. *Dalton Trans.* **2013**, *42*, 6989−7001.
(37) Song, B.; Wu, G.; Wang, Z.; Zhang, X.; Smet, M.; Dehaen, W. Metal-Ligand Coordination-Induced Self-Assembly of Bolaamphiphiles Bearing Bipyrimidine. *Langmuir* **2009**, *25*, 13306−13310.
(38) Schwab, P. F.; Fleischer, F.; Michl, J. Preparation of 5-Brominated and 5,5′-Dibrominated 2,2′-Bipyridines and 2,2′-Bipyrimidines. *J. Org. Chem.* **2002**, *67*, 443−449.
(39) Nelson, T. D.; Crouch, R. D. Cu, Ni, and Pd Mediated Homocoupling Reactions in Biaryl Syntheses: The Ullmann Reaction. *Org. React.* **2004**, *63*, 265−555.
(40) Nasielski, J.; Standaert, A.; Nasielski-Hinkens, R. Efficient Coupling of 2-Halopyrimidines to 2,2′-Bipyrimidines. *Synth. Commun.* **1991**, *21*, 901−906.
(41) Vlád, G.; Horváth, I. T. Improved Synthesis of 2,2′-Bipyrimidine. *J. Org. Chem.* **2002**, *67*, 6550−6552.
(42) Li, H.; Oppenheimer, J.; Smith, M. R.; Maleczka, R. E. Improved synthesis of electron deficient bipyridines. *Tetrahedron Lett.* **2016**, *57*, 2231−2232.
(43) Chan, K. S.; Tse, A. K.-S. Synthesis of Bis(trifluoromethyl)-2,2′-bipyridines by Nickel Catalyzed Homocoupling Reactions. *Synth. Commun.* **1993**, *23*, 1929−1934.
(44) Iyoda, M.; Otsuka, H.; Sato, K.; Nisato, N.; Oda, M. Homocoupling of Aryl Halides Using Nickel(II) Complex and Zinc in the Presence of Et_4NI. An Efficient Method for the Synthesis of Biaryls and Bipyridines. *Bull. Chem. Soc. Jpn.* **1990**, *63*, 80−87.
(45) Cordovilla, C.; Bartolomé, C.; Martínez-Ilarduya, J. M.; Espinet, P. The Stille Reaction, 38 Years Later. *ACS Catal.* **2015**, *5*, 3040−3053.
(46) Farina, V.; Krishnamurthy, V.; Scott, W. J. The Stille Reaction. *Org. React.* **1997**, *50*, 1−652.
(47) Demir, S.; Zadrozny, J. M.; Nippe, M.; Long, J. R. Exchange Coupling and Magnetic Blocking in Bipyrimidyl Radical-Bridged Dilanthanide Complexes. *J. Am. Chem. Soc.* **2012**, *134*, 18546−18549.
(48) Berg, D. J.; Boncella, J. M.; Andersen, R. A. Preparation of Coordination Compounds of Cp^*_2Yb with Heterocyclic Nitrogen Bases: Examples of Antiferromagnetic Exchange Coupling Across Bridging Ligands. *Organometallics* **2002**, *21*, 4622−4631.
(49) Goudy, V.; Jaoul, A.; Cordier, M.; Clavaguéra, C.; Nocton, G. Tuning the Stability of Pd(IV) Intermediates Using a Redox Non-innocent Ligand Combined with an Organolanthanide Fragment. *J. Am. Chem. Soc.* **2017**, *139*, 10633−10636.
(50) Wang, D.; Moutet, J.; Tricoire, M.; Cordier, M.; Nocton, G. Reactive Heterobimetallic Complex Combining Divalent Ytterbium and Dimethyl Nickel Fragments. *Inorganics* **2019**, *7*, 58−70.
(51) Day, B. M.; Guo, F.-S.; Layfield, R. A. Cyclopentadienyl Ligands in Lanthanide Single-Molecule Magnets: One Ring to Rule Them All? *Acc. Chem. Res.* **2018**, *51*, 1880−1889.
(52) Zucchi, G.; Le Goff, X. F. Magnetic properties of structurally characterized binuclear lanthanide complexes bridged by 2,2′-bipyrimidine. *Polyhedron* **2013**, *52*, 1262−1267.
(53) Visinescu, D.; Fabelo, O.; Ruiz-Pérez, C.; Lloret, F.; Julve, M. $[Fe(phen)(CN)_4]^-$: a suitable metalloligand unit to build 3d-4f heterobimetallic complexes with mixed bpym-cyano bridges (phen = 1,10 phenanthroline, bpym = 2,2′-bipyrimidine). *CrystEngComm* **2010**, *12*, 2454−2465.
(54) Geske, D. H.; Padmanabhan, G. R. An Electron Spin Resonance Study of the Anion Radicals of 9,10-Diazaphenanthrene, 2,2′-Bipyrimidine, and $\Delta^{2,2'}$-Biisobenzimidazolylidene. *J. Am. Chem. Soc.* **1965**, *87*, 1651−1655.
(55) Kaim, W.; Kohlmann, S. Four Bridging Bis Chelate Ligands with Very Low Lying π* Orbitals. MO Perturbation Calculations, Electrochemistry, and Spectroscopy of Mononuclear and Binuclear Group 6 Metal Tetracarbonyl Complexes. *Inorg. Chem.* **1987**, *26*, 68−77.
(56) Janzen, E. G. Substituent Effects on Electron Spin Resonance Spectra and Stability of Free Radicals. *Acc. Chem. Res.* **1969**, *2*, 279−288.
(57) Dust, J. M.; Arnold, D. R. Substituent Effects on Benzyl Radical ESR Hyperfine Coupling Constants. The $\sigma_\alpha\bullet$ Scale Based upon Spin Delocalization. *J. Am. Chem. Soc.* **1983**, *105*, 1221−1227.
(58) Jeon, I. R.; Park, J. G.; Xiao, D. J.; Harris, T. D. An Azophenine Radical-Bridged Fe_2 Single-Molecule Magnet with Record Magnetic Exchange Coupling. *J. Am. Chem. Soc.* **2013**, *135*, 16845−16848.
(59) Hua, C.; DeGayner, J. A.; Harris, T. D. Thiosemiquinoid Radical-Bridged Cr^{III}_2 Complexes with Strong Magnetic Exchange Coupling. *Inorg. Chem.* **2019**, *58*, 7044−7053.
(60) Kanetomo, T.; Yoshitake, T.; Ishida, T. Strongest Ferromagnetic Coupling in Designed Gadolinium(III)-Nitroxide Coordination Compounds. *Inorg. Chem.* **2016**, *55*, 8140−8146.
(61) Kanetomo, T.; Ishida, T. Strongest Exchange Coupling in Gadolinium(III) and Nitroxide Coordination Compounds. *Inorg. Chem.* **2014**, *53*, 10794−10796.
(62) Thorarinsdottir, A. E.; Bjornsson, R.; Harris, T. D. Insensitivity of Magnetic Coupling to Ligand Substitution in a Series of Tetraoxolene Radical-Bridged Fe_2 Complexes. *Inorg. Chem.* **2020**, *59*, 4634−4649.
(63) Finn, C. B. P.; Orbach, R.; Wolf, W. P. Spin-Lattice Relaxation in Cerium Magnesium Nitrate at Liquid Helium Temperatures: A New Process. *Proc. Phys. Soc., London* **1961**, *77*, 261−268.
(64) Chibotaru, L. F.; Iwahara, N. Ising exchange interaction in lanthanides and actinides. *New J. Phys.* **2015**, *17*, 103028.
(65) Prša, K.; Nehrkorn, J.; Corbey, J. F.; Evans, W. J.; Demir, S.; Long, J. R.; Guidi, T.; Waldmann, O. Perspectives on Neutron Scattering in Lanthanide-Based Single-Molecule Magnets and a Case Study of the $Tb_2(\mu\text{-}N_2)$ System. *Magnetochemistry* **2016**, *2*, 45−63.
(66) Kofu, M.; Yamamuro, O.; Kajiwara, T.; Yoshimura, Y.; Nakano, M.; Nakajima, K.; Ohira-Kawamura, S.; Kikuchi, T.; Inamura, Y. Hyperfine structure of magnetic excitations in a Tb-based single-molecule magnet studied by high-resolution neutron spectroscopy. *Phys. Rev. B: Condens. Matter Mater. Phys.* **2013**, *88*, 064405−064407.
(67) Baker, M. L.; Tanaka, T.; Murakami, R.; Ohira-Kawamura, S.; Nakajima, K.; Ishida, T.; Nojiri, H. Relationship Between Torsion and

https://dx.doi.org/10.1021/jacs.0c10612
J. Am. Chem. Soc. XXXX, XXX, XXX−XXX

Anisotropic Exchange Coupling in a Tb^{III}-Radical-Based Single-Molecule Magnet. *Inorg. Chem.* **2015**, *54*, 5732−5738.
(68) Vieru, V.; Iwahara, N.; Ungur, L.; Chibotaru, L. F. Giant exchange interaction in mixed lanthanides. *Sci. Rep.* **2016**, *6*, 24046.
(69) Zhang, Y.-Q.; Luo, C.-L.; Wang, B.-W.; Gao, S. Understanding the Magnetic Anisotropy in a Family of N_2^{3-} Radical-Bridged Lanthanide Complexes: Density Functional Theory and ab Initio Calculations. *J. Phys. Chem. A* **2013**, *117*, 10873−10880.
(70) Zhang, Y.-Q.; Luo, C.-L.; Zhang, Q. Exchange coupling and magnetic anisotropy in a family of bipyrimidyl radical-bridged dilanthanide complexes: Density functional theory and ab initio calculations. *J. Comput. Chem.* **2014**, *35*, 904−909.
(71) Langley, S. K.; Wielechowski, D. P.; Vieru, V.; Chilton, N. F.; Moubaraki, B.; Abrahams, B. F.; Chibotaru, L. F.; Murray, K. S. A $\{Cr(III)_2Dy(III)_2\}$ single-molecule magnet: enhancing the blocking temperature through 3d magnetic exchange. *Angew. Chem., Int. Ed.* **2013**, *52*, 12014−12019.
(72) Gould, C. A.; Darago, L. E.; Gonzalez, M. I.; Demir, S.; Long, J. R. A Trinuclear Radical-Bridged Lanthanide Single-Molecule Magnet. *Angew. Chem., Int. Ed.* **2017**, *56*, 10103−10107.
(73) Zhang, P.; Perfetti, M.; Kern, M.; Hallmen, P. P.; Ungur, L.; Lenz, S.; Ringenberg, M. R.; Frey, W.; Stoll, H.; Rauhut, G.; van Slageren, J. Exchange coupling and single molecule magnetism in redox-active tetraoxolene-bridged dilanthanide complexes. *Chem. Sci.* **2018**, *9*, 1221−1230.
(74) Demir, S.; Nippe, M.; Gonzalez, M. I.; Long, J. R. Exchange coupling and magnetic blocking in dilanthanide complexes bridged by the multi-electron redox active ligand 2,3,5,6-tetra(2-pyridyl)pyrazine. *Chem. Sci.* **2014**, *5*, 4701−4711.
(75) Guo, F.-S.; Layfield, R. A. Strong direct exchange coupling and single-molecule magnetism in indigo-bridged lanthanide dimers. *Chem. Commun.* **2017**, *53*, 3130−3133.
(76) Demir, S.; Zadrozny, J. M.; Long, J. R. Large Spin-Relaxation Barriers for the Low-Symmetry Organolanthanide Complexes $[Cp^*_2Ln(BPh_4)]$ (Cp*=pentamethylcyclopentadienyl; Ln = Tb, Dy). *Chem. - Eur. J.* **2014**, *20*, 9524−9529.
(77) Evans, W. J.; Davis, B. L.; Champagne, T. M.; Ziller, J. W. C-H bond activation through steric crowding of normally inert ligands in the sterically crowded gadolinium and yttrium $(C_5Me_5)_3M$ complexes. *Proc. Natl. Acad. Sci. U. S. A.* **2006**, *103*, 12678−12683.
(78) Johnson, T. B.; Joyce, W. A. Researches on Pyrimidines. LXXVI. New Methods of Synthesizing 2-Ketopyrimidines and Their Sulfur Analogs. *J. Am. Chem. Soc.* **1915**, *37*, 2151−2164.
(79) Baram, S. G.; Shkurko, O. P.; Mamaev, V. P. Pyrimidines. IX. Synthesis of 5-Substituted 2-Fluoropyrimidines. *Izv. Sib. Otd. An. Khim.* **1977**, *1*, 106−109.
(80) *wSAINT and APEX 2 Software for CCD Diffractometers*; Bruker AXS Inc.: Madison, WI, 2014.
(81) Sheldrick, G. M. *SADABS*, Version 2.03, Bruker Analytical X-Ray Systems, Inc.: Madison, WI, 2000.
(82) Sheldrick, G. M. *TWINABS.*; University of Göttingen: Göttingen, Germany, 2009.
(83) Rigaku Oxford Diffraction *CrysAlisPro Software system*, version 1.171.39.7a; Rigaku Corporation: Oxford, U.K., 2015
(84) Sheldrick, G. M. SHELXT-Integrated Space-Group and Crystal-Structure Determination. *Acta Crystallogr., Sect. A: Found. Adv.* **2015**, *71*, 3−8.
(85) Sheldrick, G. M. A Short History of SHELX. *Acta Crystallogr., Sect. A: Found. Crystallogr.* **2008**, *64*, 112−122.
(86) Dolomanov, O. V.; Bourhis, L. J.; Gildea, R. J.; Howard, J. A. K.; Puschmann, H. OLEX2: A Complete Structure Solution, Refinement and Analysis Program. *J. Appl. Crystallogr.* **2009**, *42* (2), 339−341.
(87) Chilton, N. F.; Anderson, R. P.; Turner, L. D.; Soncini, A.; Murray, K. S. PHI: a powerful new program for the analysis of anisotropic monomeric and exchange-coupled polynuclear d- and f-block complexes. *J. Comput. Chem.* **2013**, *34*, 1164−1175.
(88) Reta, D.; Chilton, N. F. Uncertainty estimates for magnetic relaxation times and magnetic relaxation parameters. *Phys. Chem. Chem. Phys.* **2019**, *21*, 23567−23575.
(89) Evans, P.; Reta, D.; Whitehead, G. F. S.; Chilton, N. F.; Mills, D. P. Bis-Monophospholyl Dysprosium Cation Showing Magnetic Hysteresis at 48 K. *J. Am. Chem. Soc.* **2019**, *141*, 19935−19940.
(90) Aquilante, F.; Autschbach, J.; Carlson, R. K.; Chibotaru, L. F.; Delcey, M. G.; De Vico, L.; Fdez Galván, I.; Ferré, N.; Frutos, L. M.; Gagliardi, L.; Garavelli, M.; Giussani, A.; Hoyer, C. E.; Li Manni, G.; Lischka, H.; Ma, D.; Malmqvist, P. Å.; Müller, T.; Nenov, A.; Olivucci, M.; Pedersen, T. B.; Peng, D.; Plasser, F.; Pritchard, B.; Reiher, M.; Rivalta, I.; Schapiro, I.; Segarra-Martí, J.; Stenrup, M.; Truhlar, D. G.; Ungur, L.; Valentini, A.; Vancoillie, S.; Veryazov, V.; Vysotskiy, V. P.; Weingart, O.; Zapata, F.; Lindh, R. MOLCAS 8: New capabilities for multiconfigurational quantum chemical calculations across the periodic table. *J. Comput. Chem.* **2016**, *37*, 506−541.
(91) Chibotaru, L. F.; Ungur, L. Ab initio calculation of anisotropic magnetic properties of complexes. I. Unique definition of pseudospin Hamiltonians and their derivation. *J. Chem. Phys.* **2012**, *137*, 064112.
(92) Chibotaru, L. F.; Ungur, L.; Aronica, C.; Elmoll, H.; Pilet, G.; Luneau, D. Structure, Magnetism, and Theoretical Study of a Mixed-Valence $Co^{II}_3Co^{III}_4$ Heptanuclear Wheel: Lack of SMM Behavior Despite Negative Magnetic Anisotropy. *J. Am. Chem. Soc.* **2008**, *130*, 12445−12455.
(93) Chibotaru, L. F.; Ungur, L.; Soncini, A. The origin of nonmagnetic Kramers doublets in the ground state of dysprosium triangles: evidence for a toroidal magnetic moment. *Angew. Chem., Int. Ed.* **2008**, *47*, 4126−4129.
(94) Shoji, M.; Koizumi, K.; Kitagawa, Y.; Kawakami, T.; Yamanaka, S.; Okumura, M.; Yamaguchi, K. A general algorithm for calculation of Heisenberg exchange integrals J in multispin systems. *Chem. Phys. Lett.* **2006**, *432*, 343−347.
(95) Neese, F. The ORCA program system. *Wiley Interdiscip. Rev.: Comput. Mol. Sci.* **2012**, *2*, 73−78.

https://dx.doi.org/10.1021/jacs.0c10612
J. Am. Chem. Soc. XXXX, XXX, XXX−XXX